AD-A031 011 ALABAMA UNIV IN HUNTSVILLE SCHOOL OF GRADUATE STUDIE--ETC F/G 20/5
THEORETICAL INVESTIGATION OF THE LASER AMPLIFICATION PROPERTIES--ETC(U)
JUL 76 W B MCKNIGHT, C H CHAN DAAH01-75-C-0911
UNCLASSIFIED UAH-RR-189 NL

1 OF 1
ADA031011

END
DATE
FILMED
11-76

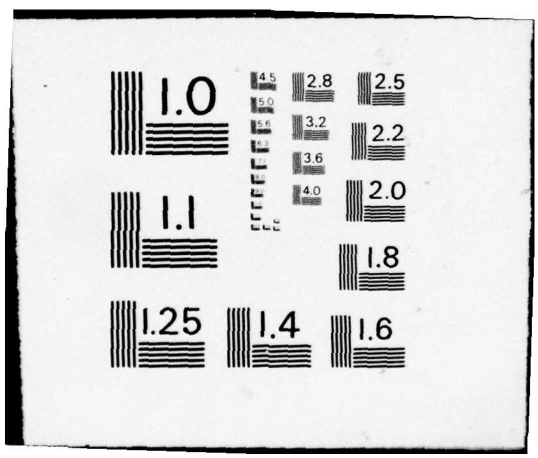
1.0
4.5
5.0
5.6
2.8
3.2
3.6
4.0
2.5
2.2
2.0
1.1
1.8
1.25
1.4
1.6

FG.

(12)

UAH Research Report No. 189

THEORETICAL INVESTIGATION OF THE LASER AMPLIFICATION PROPERTIES OF A CONTINUOUS WAVE, ELECTRICAL DISCHARGE LASER (CW-EDL)

Final Report - Contract DAAH01-75-C-0911

Prepared by:

W. B. McKnight

C. H. Chan

Division of Graduate Studies and Research
The University of Alabama in Huntsville
P. O. Box 1247
Huntsville, Alabama 35807

Prepared for:

U.S. Army Missile Command
Redstone Arsenal, Alabama 35809

July 1976

DISPOSITION INSTRUCTIONS

DESTROY THIS REPORT WHEN IT IS NO LONGER NEEDED. DO NOT RETURN IT TO THE ORIGINATOR.

DISCLAIMER

THE FINDINGS IN THIS REPORT ARE NOT TO BE CONSTRUED AS AN OFFICIAL DEPARTMENT OF THE ARMY POSITION UNLESS SO DESIGNATED BY OTHER AUTHORIZED DOCUMENTS.

TRADE NAMES

USE OF TRADE NAMES OR MANUFACTURERS IN THIS REPORT DOES NOT CONSTITUTE AN OFFICIAL INDORSEMENT OR APPROVAL OF THE USE OF SUCH COMMERCIAL HARDWARE OR SOFTWARE.

UAH Research Report No. 189

THEORETICAL INVESTIGATION OF THE LASER AMPLIFICATION PROPERTIES OF A CONTINUOUS WAVE, ELECTRICAL DISCHARGE LASER (CW-EDL)

Final Report - Contract DAAH01-75-C-0911

Prepared by:

W. B. McKnight

C. H. Chan

407 648

Sch

Division of Graduate Studies and Research
The University of Alabama in Huntsville
P. O. Box 1247
Huntsville, Alabama 35807

Prepared for:

U.S. Army Missile Command
Redstone Arsenal, Alabama 35809

July 1976

DISPOSITION INSTRUCTIONS

DESTROY THIS REPORT WHEN IT IS NO LONGER NEEDED. DO NOT RETURN IT TO THE ORIGINATOR.

DISCLAIMER

THE FINDINGS IN THIS REPORT ARE NOT TO BE CONSTRUED AS AN OFFICIAL DEPARTMENT OF THE ARMY POSITION UNLESS SO DESIGNATED BY OTHER AUTHORIZED DOCUMENTS.

TRADE NAMES

USE OF TRADE NAMES OR MANUFACTURERS IN THIS REPORT DOES NOT CONSTITUTE AN OFFICIAL INDORSEMENT OR APPROVAL OF THE USE OF SUCH COMMERCIAL HARDWARE OR SOFTWARE.

UNCLASSIFIED

SECURITY CLASSIFICATION OF THIS PAGE (When Data Entered)

REPORT DOCUMENTATION PAGE		READ INSTRUCTIONS BEFORE COMPLETING FORM
1. REPORT NUMBER UAH Research Report No. 189	2. GOVT ACCESSION NO.	3. RECIPIENT'S CATALOG NUMBER
4. TITLE (and Subtitle) Theoretical Investigation of the Laser Amplification Properties of a Continuous Wave, Electrical Discharge Laser (CW-EDL)		5. TYPE OF REPORT & PERIOD COVERED Final Report May 1975 – July 1976
		6. PERFORMING ORG. REPORT NUMBER UAH Research Report No. 189
7. AUTHOR(s) W. B. McKnight C. H. Chan UAH-RR-189		8. CONTRACT OR GRANT NUMBER(s) ~~Contract~~ DAAH01-75-C-0911 NEW
9. PERFORMING ORGANIZATION NAME AND ADDRESS The University of Alabama in Huntsville P. O. Box 1247, Huntsville AL 35807		10. PROGRAM ELEMENT, PROJECT, TASK AREA & WORK UNIT NUMBERS
11. CONTROLLING OFFICE NAME AND ADDRESS Commander, U. S. Army Missile Command Redstone Arsenal AL 35809 Attention: AMSMI-IPWC		12. REPORT DATE July 1976
		13. NUMBER OF PAGES 59
14. MONITORING AGENCY NAME & ADDRESS (if different from Controlling Office) 65p.		15. SECURITY CLASS. (of this report) UNCLASSIFIED
		15a. DECLASSIFICATION/DOWNGRADING SCHEDULE

16. DISTRIBUTION STATEMENT (of this Report)

Approved for public release - distribution unlimited

17. DISTRIBUTION STATEMENT (of the abstract entered in Block 20, if different from Report)

18. SUPPLEMENTARY NOTES

19. KEY WORDS (Continue on reverse side if necessary and identify by block number)

Laser, resonator, laser amplifier, mode-media interaction

20. ABSTRACT (Continue on reverse side if necessary and identify by block number)

A rigorously-derived paraxial approximation based on scaling the coordinates of the wave equation in terms of natural parameters of the system under consideration was used to study the behavior of a continuous-wave electric discharge (CW-EDL) laser medium considered as an

DD FORM 1 JAN 73 1473 EDITION OF 1 NOV 65 IS OBSOLETE
S/N 0102-014-6601

UNCLASSIFIED 407 648

SECURITY CLASSIFICATION OF THIS PAGE (When Data Entered)

amplifier for the effects of diffraction, saturation, and detuning of the operating frequency from the center of the gain line, on the quality of the propagating beam. Computer-generated results showed no serious beam degradation from these effects was to be expected in the system when treated as an amplifier. This formulation was then used, subject to the constraints of the unstable resonator optical cavity, to treat the system as an oscillator, assuming cylindrical symmetry in the loaded resonator. Near-field phase and intensity patterns were obtained by computer, and used to generate far-field patterns. This computer-modelling of the unstable resonator with continuous gain medium is compared to computer models developed by others.

ABSTRACT

A rigorously-derived paraxial approximation based on scaling the coordinates of the wave equation in terms of natural parameters of the system under consideration was used to study the behavior of a continuous-wave electric discharge (CW-EDL) laser medium considered as an amplifier for the effects of diffraction, saturation, and detuning of the operating frequency from the center of the gain line, on the quality of the propagating beam. Computer-generated results showed no serious beam degradation from these effects was to be expected in the system when treated as an amplifier. This formulation was then used, subject to the constraints of the unstable resonator optical cavity, to treat the system as an oscillator, assuming cylindrical symmetry in the loaded resonator. Near-field phase and intensity patterns were obtained by computer, and used to generate far-field patterns. This computer-modelling of the unstable resonator with continuous gain medium is compared to computer models developed by others.

I. INTRODUCTION

This research had as its main objective a formulation of the equations for propagating electromagnetic waves in a laser medium in order to study the properties and behavior of the laser beam in gas laser systems, such as the CW-EDL, that have substantial gain. This study of these beam characteristics and factors affecting them is useful in the establishment of design or operational modifications that could lead to improved far-field intensities for the laser output or to explanations of unexpected beam degradation in terms of laser media or laser resonator characteristics.

In order to investigate the properties of amplifying media of gas lasers relating to beam quality, the application of a rigorously-derived paraxial approximation[1] to the wave equation for propagation through an amplifying medium was necessary. Laser beam quality in the device is a critical parameter, along with atmospheric propagation, in determining the far-field intensity pattern. Factors important for beam quality are diffraction due to finite beam size, beam distortion due to saturation of the medium gain, and refraction and defocussing due to a difference in frequency between the laser frequency and the center of the gain line. While Bridges[2] has shown the effect of saturation on propagation in an amplifying medium, the other effects have not been studied in depth. After derivation of the equations, they are solved numerically on a computer, and results of gas lasers with various choices of the important parameters are plotted. The shapes of the curves are then used to determine beam distortion as a function of the various parameters.

As the result of studying these curves, it is found that for lasers with media of the general characteristics of the CW-EDL, these factors of saturation and detuning are of minor importance where the system is treated as an amplifier; however, further consideration indicates that treatment of the system as an amplifier is not adequate, and in particular, diffraction may be of significant importance in the case of an active medium in a resonator. On the other hand, detuning is very likely to be of minor importance in the resonator case, as even though the system is disturbed sufficiently to shift its operating frequency from line center, it will quickly readjust so that the detuning is small.

After investigation of the properties of an amplifier, the equations were then set up for a typical CW-EDL system configured as an oscillator using a positive-branch, confocal unstable resonator. The laser system was assumed to have cylindrical symmetry in the gain medium for the purposes of this study.

II. EQUATIONS OF PROPAGATION

Standard practice in theoretical work on propagation in laser amplifiers[3] and in the study of modes in spherical resonators[4] has depended on certain assumptions and approximations that lead to an inconsistency. Specifically, it is assumed that the electric field is plane polarised in the x direction. According to the exact Maxwell's equations, this then means that the field is independent of x. However, when the resulting equations are solved in the paraxial approximation, gaussian solutions are found in the transverse direction, which is indeed in accordance with experiment, in spite of the fact that the transverse derivative of the field is shown to be zero by the exact equations. The paraxial approximation has been analyzed to resolve the inconsistency and the resulting equations then were solved numerically to yield quantitative results.

For waves propagating in the z(axial) direction one may write the field as

$$\vec{\mathcal{E}} = \vec{\mathcal{E}}_T + \hat{a}\,\mathcal{E}_z \equiv e^{ikz}\,(\vec{F}_T + \hat{a}_z F_z) \tag{2.1}$$

where the subscript T indicates the transverse part of the field and $\hat{a}_z$ is a unit vector in the z direction. Let the total gradient be

$$\nabla = \nabla_T + \hat{a}_z \frac{\partial}{\partial z} \tag{2.2}$$

where ∇_T represents the transverse gradient. One now takes the curl of both sides of the Maxwell equation curl $\vec{\mathcal{E}} = i\omega\mu_o \vec{H}$ (2.3)

and using the relation curl $\vec{H} = -i\omega\varepsilon_o \kappa \vec{\mathcal{E}}$ (2.4)

one obtains curl curl $\vec{\mathcal{E}} = (\omega/c)^2 \kappa \vec{\mathcal{E}}$ (2.5)

where ω is the angular frequency and $\kappa \equiv \left(\frac{\varepsilon}{\varepsilon_o}\right) + i\left(\frac{\sigma}{\omega\varepsilon_o}\right)$ where ε is the

dielectric constant and σ is the specific conductivity. Using (2.1) and (2.2) in (2.5) the transverse and longitudinal components of the field are obtained:

$$\nabla_T \left(\nabla_T \cdot \vec{F}_T + \frac{\partial F_z}{\partial z} + ikF_z\right) - \nabla_T^2 \vec{F}_T - \frac{\partial^2 \vec{F}_T}{\partial z^2} - 2ik \frac{\partial \vec{F}_T}{\partial z}$$

$$+ k^2 \vec{F}_T = \left(\frac{\omega}{c}\right)^2 \kappa \vec{F}_T \tag{2.6}$$

$$\frac{\partial}{\partial z} (\nabla_T \cdot \vec{F}_T) + ik\nabla_T \cdot \vec{F}_T - \nabla_T^2 F_z = \left(\frac{\omega}{c}\right)^2 \kappa F_z \tag{2.7}$$

Consider a beam of width w_o in the transverse dimension. It has associated with it a diffraction length $\ell = kw_o^2 = \frac{2\pi}{\lambda} w_o^2$ where λ is the wavelength. These characteristic dimensions may then be used to scale (2.6) and (2.7)

$$\text{Let } x = w_o\xi, \quad y = w_o\eta, \quad z = \ell\zeta \tag{2.8}$$

Since in the problem to be considered $w_o << \ell$, let

$$f \equiv \frac{w_o}{\ell} = \frac{1}{kw_o} \tag{2.9}$$

Using (2.8) and (2.9) in (2.6) and (2.7) one obtains

$$\nabla_\tau \left(f\nabla_\tau \cdot \vec{F}_\tau + f^2 \frac{\partial F_\zeta}{\partial \zeta} + iF_\zeta\right) - f\nabla_\tau^2 \vec{F}_\tau - f^3 \frac{\partial^2 \vec{F}_\tau}{\partial \zeta^2}$$

$$- 2if \frac{\partial \vec{F}_\tau}{\partial \zeta} = f\left[\left(\omega \frac{w_o}{c}\right)^2 \kappa - \left(kw_o\right)^2\right] \vec{F}_\tau \tag{2.10}$$

$$f^3 \frac{\partial}{\partial \zeta} (\nabla_\tau \cdot \vec{F}_\tau) + if\nabla_\tau \cdot \vec{F}_\tau - f^2 \nabla_\tau F_\zeta = f^2\left(\omega \frac{w_o}{c}\right)^2 \kappa F_\zeta \tag{2.11}$$

where $\vec{F}_T\,(\vec{r}_T, z) \rightarrow \vec{F}_\tau\,(\vec{\rho}, \zeta)$, $F_z\,(\vec{r}_T, z) \rightarrow F_\zeta(\vec{\rho}, \zeta)$ (2.12)

and $$\nabla_\tau \equiv \hat{a}_x \frac{\partial}{\partial \xi} + \hat{a}_y \frac{\partial}{\partial \eta} \tag{2.13}$$

with $\hat{a}_x$ and $\hat{a}_y$ unit vectors in the x and y directions.

The dielectric response, κ, of a medium with n atoms per unit volume may be written as

$$\kappa = \kappa_L + \frac{(\Omega - i)\left[\sqrt{\kappa_L}\,(cg/\omega)\right]}{1 + \Omega^2 + I} \tag{2.14}$$

$$\equiv \kappa_L + \left[\sqrt{\kappa_L}\,(cg/\omega)\right] m\left(\omega, |F|^2\right) \tag{2.15}$$

where $\Omega = (\omega - \omega_{ab})/\gamma_{ab}$ is the fractional detuning of the frequency from the center of the gain line, κ_L is the background linear dielectric constant, g is the small signal gain, and $I = |F|^2/F_s^2$ is the field intensity in units of the saturation intensity. Choosing

$$k^2 = (\omega/c)^2\,\kappa_L \tag{2.16}$$

equations (2.10) and (2.11) reduce to

$$\nabla_\tau\,(f\nabla_\tau \cdot \vec{F}_T + f^2 \frac{\partial F_\zeta}{\partial \zeta} + iF_\zeta) - f\nabla_\tau^2\,\vec{F}_\tau - f^3\,\frac{\partial^2 \vec{F}_\tau}{\partial \zeta^2}$$
$$- 2\,if\,\frac{\partial \vec{F}_\tau}{\partial \zeta} = (fg\ell m)\,\vec{F}_\tau \tag{2.17}$$

$$f^3 \frac{\partial}{\partial \zeta}\,(\nabla_\tau \cdot \vec{F}_\tau) + if\nabla_\tau \cdot \vec{F}_\tau - f^2\nabla_\tau^2\,F_\zeta = \left[1 + (f^2 g\ell m)\right] F_\zeta \tag{2.18}$$

As in physical problems of interest $f^2 g\ell = g/k$ = the gain in a distance k^{-1} is always small, one may obtain a consistent solution by expanding the field in powers of f. Using only alternate powers one has

for the transverse and longitudinal field components

$$\vec{F}_\tau = \vec{F}_\tau^{(0)} + f^2 \vec{F}_\tau^{(2)} + \ldots \tag{2.19}$$

$$\vec{F}_\zeta + fF_\zeta^{(1)} + f^3 F_\zeta^{(3)} + \ldots \tag{2.20}$$

It may be noted that (2.18) contains no zero-order terms. Also, since m is a function of $|F|^2$, it must be expanded in powers of f. On using (2.20) with (2.18) to first order in f

$$F_\zeta^{(1)} = i\nabla_\tau \cdot F_\tau^{(0)} \tag{2.21}$$

from which it is seen that in first order a small longitudinal component of the field is present.

Using (2.19) with (2.17) the lowest-order terms are

$$\nabla_\tau^2 \vec{F}_\tau^{(0)} + 2i\left(\frac{\partial F_\tau^{(0)}}{\partial \zeta}\right) = -(g\,\ell)\, m_o \vec{F}_\tau^{(0)} \tag{2.22}$$

$$\text{where } m_o \equiv m\left(|\vec{F}^{(0)}|^2\right) = \frac{\Omega - i}{1 + \Omega^2 + I^{(0)}} \tag{2.23}$$

This resolves the inconsistency since to lowest order the field is transverse and may depend on the transverse coordinate.

Plane polarized solutions of the form

$$\vec{F}_\tau^{(0)} = \vec{E}e^{iS} \tag{2.24}$$

may now be sought where E and the phase S are real. Substituting (2.24) in (2.22) and equating real and imaginary parts, one has

$$\nabla_\tau^2 \vec{E} - (\nabla_\tau S)^2 \vec{E} - 2\left(\frac{\partial S}{\partial \zeta}\right) \vec{E} = -(g\,\ell)\ (\text{Re } m_o)\ \vec{E} \tag{2.25}$$

$$2\ (\nabla_\tau S \cdot \nabla_\tau)\vec{E} + \nabla_\tau^2\, S\vec{E} + 2\left(\frac{\partial \vec{E}}{\partial \zeta}\right) = -\ (g\,\ell)\ (\text{Im } m_o)\ \vec{E} \tag{2.26}$$

taking the scalar product of both sides of (2.25) and (2.26) with $\vec{E}$

one obtains

$$(\nabla_\tau S)^2 + 2\left(\frac{\partial S}{\partial \zeta}\right) = (g\,\ell)\ (\mathrm{Re}\ m_o) + \left(\vec{E} \cdot \nabla_\tau{}^2 \vec{E}\right) E^{-2} \tag{2.27}$$

$$\nabla_\tau \cdot (E^2 \nabla_\tau S) + \left(\frac{\partial E^2}{\partial \zeta}\right) = -(g\,\ell)\ (\mathrm{Im}\ m_o)\ E^2 \tag{2.28}$$

Rays normal to surfaces of constant phase obey the equation

$$\frac{d\vec{r}_T}{ds} = \frac{\nabla_T S}{|\nabla(S + kz)|} \tag{2.29}$$

$$\frac{dz}{ds} = \frac{k + (\partial S/\partial z)}{|\nabla(S + kz)|} \tag{2.30}$$

and dividing (2.29) by (2.30) gives

$$\frac{d\vec{r}_T}{dz} = \frac{\nabla_T S}{k + \partial S/\partial z} \tag{2.31}$$

In the scaled variables $\vec{r}_T = w_o \vec{\rho}$ and $z = \zeta\ell$. This becomes

$$\frac{d\vec{\rho}}{d\zeta} = \frac{\nabla_\tau S}{1 + f^2 (\partial S/\partial \zeta)} \tag{2.32}$$

and neglecting the second order term in f

$$\frac{d\vec{\rho}}{d\zeta} = \nabla_\tau S \tag{2.33}$$

III. NUMERICAL SOLUTION

In cylindrical coordinates equations (2.27), (2.28), and (2.33) become

$$\left(\frac{\partial S}{\partial \rho}\right)^2 + \frac{1}{\rho^2}\left(\frac{\partial S}{\partial \phi}\right)^2 + 2\left(\frac{\partial S}{\partial \zeta}\right) = g\,\ell\,\mathrm{Re}\,m_o + \frac{1}{\rho\sqrt{I}}\frac{\partial}{\partial \rho}\left(\rho\frac{\partial\sqrt{I}}{\partial \rho}\right) + \frac{1}{\rho^2\sqrt{I}}\frac{\partial^2\sqrt{I}}{\partial \phi^2}$$

$$\frac{1}{\rho}\frac{\partial}{\partial \rho}\left(I\rho\frac{\partial S}{\partial \rho}\right) + \frac{1}{\rho^2}\frac{\partial}{\partial \phi}\left(I\frac{\partial}{\partial \phi}\right) + \frac{\partial I}{\partial \zeta} = -\,g\ell\,I\,\mathrm{Im}\,m_o$$

$$\frac{d\rho}{d\zeta} = \frac{\partial S}{\partial \rho}\,,\quad \rho^2\frac{d\phi}{d\zeta} = \frac{\partial S}{\partial \phi}$$

For an azimuthally symmetric amplifier, these equations reduce to

$$\frac{d\rho}{d\zeta} = \frac{\partial S}{\partial \rho} \tag{3.1}$$

$$\frac{1}{\rho}\frac{\partial}{\partial \rho}\left(I\rho\frac{\partial}{\partial \rho}\right) + \frac{\partial I}{\partial \zeta} = -\,g\ell\,I\,\mathrm{Im}\,m_o \tag{3.2}$$

$$\left(\frac{\partial S}{\partial \rho}\right)^2 + 2\left(\frac{\partial S}{\partial \zeta}\right) = g\ell\,\mathrm{Re}\,m_o + \frac{1}{\rho\sqrt{I}}\frac{\partial}{\partial \rho}\left(\rho\frac{\partial\sqrt{I}}{\partial \rho}\right) \tag{3.3}$$

where ρ is the radical distance normalized to the beam size w_o, ζ is the axial distance normalized to the diffraction length ℓ, I is the beam intensity normalized to the saturation intensity. S is the phase and g is the small signal gain per unit length and $m_o = \dfrac{\Omega - i}{1 + \Omega^2 + I}$ for a homogeneously broadened system. Ω is the fractional detuning of the operating frequency from line center.

To solve these equations, we introduce the beam slope

$$v = \frac{d\rho}{d\zeta} \tag{3.4}$$

and use it to eliminate S in Eqs. (3.2) and (3.3)

$$\frac{1}{\rho}\frac{\partial}{\partial\rho}(I\rho v) + \frac{\partial I}{\partial\zeta} = -\, g\ell\, I\, \mathrm{Im}\, m_o \qquad (3.5)$$

$$\frac{\partial}{\partial\rho}(v^2) + 2\frac{\partial v}{\partial\zeta} = \frac{\partial}{\partial\rho}(g\ell\ \mathrm{Re}\ m_o) + \left[\frac{\partial}{\partial\rho}\frac{1}{\rho\sqrt{I}}\frac{\partial}{\partial\rho}\left(\rho\frac{\partial\sqrt{I}}{\partial\rho}\right)\right] \qquad (3.6)$$

with

$$\frac{dI}{d\zeta} = \frac{\partial I}{\partial\zeta} + v\frac{\partial I}{\partial\rho}$$

and

$$\frac{dv}{d\zeta} = \frac{\partial v}{\partial\zeta} + v\frac{\partial v}{\partial\rho}$$

Eqs. (3.5) and (3.6) reduce to

$$\frac{dI}{d\zeta} = -\, g\ell\, I\, \mathrm{Im}\, m_o - I\frac{v}{\rho} - I\frac{\partial v}{\partial\rho} \qquad (3.7)$$

$$\frac{dv}{d\zeta} = \frac{1}{4}\frac{\partial p}{\partial\rho} \qquad (3.8)$$

where

$$p = \frac{1}{2}G^2 + \frac{\partial G}{\partial\rho} + \frac{G}{\rho} + 2\, g\ell\ \mathrm{Re}\ m_o$$

$$G = \frac{\partial}{\partial\rho}(\ell n\ I)$$

Eqs. (3.4), (3.7) and (3.8) are the basic equations. They can be integrated numerically step by step in the ζ-direction along the path of a ray.

In an amplifying system, the incident beam is usually given at the incident plane, e.g. both the beam intensity and the beam slope are given as a function of ρ at $\zeta = 0$. Also along the axis of the amplifier, the beam slope is zero and the beam intensity must be either at a

maximum or at a minimum, e.g. both $v = 0$ and $G = 0$ at $\rho = 0$ for all values of ζ. With these initial conditions, Eqs. (3.4), (3.7) and (3.8) can be evaluated.

The numerical procedure used is to first divide the beam at the incident plane into a number of rays at equal distances along the ρ-direction and integrate ρ, I, and v along each ray step-by-step in the ζ direction. The method used here is a Predictor-Corrector Method. Assuming that ρ, I and v are known in the ζ_{n-1} and ζ_n planes, one first estimates a tentative value of ρ_{n+1}, the prediction, in the ζ_{n+1} plane by

$$\rho_{n+1} = \rho_{n-1} + 2\Delta\zeta \left(\frac{\partial \rho}{\partial \zeta}\right)_n$$

where $\Delta\zeta$ is the integration step and $\left(\frac{\partial \rho}{\partial \zeta}\right)_n = v_n$ from Eq. (3.4), (similarly, for the other two quantities I and v). One then calculates a corrector

$$\rho_{n+1} = \rho_n + \frac{\Delta\zeta}{2} \left[\left(\frac{\partial \rho}{\partial \zeta}\right)'_{n+1} + \left(\frac{\partial \rho}{\partial \zeta}\right)_n \right]$$

where $\left(\frac{\partial \rho}{\partial \zeta}\right)'_{n+1} = \bar{v}_{n+1}$ calculated from the predicted value. If the difference between the corrector and predictor is within a small preassigned tolerance, one stops the iteration and moves to the next plane; otherwise the calculation is repeated using the corrector as the predictor and recalculating a corrector.

This method is used throughout the integration along the ζ direction. For the first integration from the incident plane to the first plane, the extrapolated values ρ_{n-1}, I_{n-1}, v_{n-1} were used to calculate

the first predictors.

In evaluating the right hand sides of Eqs. (3.7) and (3.8), partial derivatives of various quantities with respect to ρ are required. These are obtained by fitting a quadratic curve to values at three nearest points to the point where the derivative is needed. The derivative is taken to be the tangent to this curve.

This numerical procedure as stated can be applied to almost any form of the incident beam. In the following, consideration is restricted to an incident collimated Gaussian beam. Such a beam is characterized by two parameters, I_o and w_o, where I_o is the peak intensity in units of saturation intensity and w_o is the beam size defined to be that at which the beam intensity falls to $\frac{1}{e^2}$ of I_o. Two different values for w_o = 2.5 cm, 5.0 cm and three for I_o = 0.1, 0.25, 0.5 were considered in the calculation. In a typical calculation, 41 rays are taken, the interval between successive rays at the incident plane is taken as 0.05 w_o. The number of steps in integration along the ζ direction are 100 to 400 depending on the length of the amplifier in consideration. A sample program written in Fortran IV for the Univac 1108 system is listed in the appendix 1. It requires approximately 20-30 seconds for a single calculation. Figures 1-18 are the result of this calculation. The various inputs are

I_o = 0.1, 0.25, 0.5

w_o = 2.5, 5.0 cm

g = 0.01/cm

Ω = 0.0, 0.1, 0.5

L = 100, 200, 400 cm

where L is the length of the amplifier. In these figures, the amplified beams at the output plane are normalized to their values on the amplifier axis to make the distortion more evident. These normalization constants for various inputs are listed in Table I. For example, for $I_o = 0.25$, $w_o = 2.5$ cm, $\Omega = 0.5$, $L = 400$ cm, the amplified intensity along the axis at the output plane is 1.782 in units of saturation intensity or an amplification of 7.13 times of the incident intensity. The output intensity distribution for this case is given in Figure 6 as the outmost curve. In Figures 1-18, for the sake of comparison, the input gaussian distributions are also presented. As may be seen in every figure, the longer the amplifier, the larger the distortion away from the gaussian distribution. The amount of distortion is virtually independent of the beam size, w_o, but dependent on the incident intensity, I_o, and the detuning, Ω. The distortion is large for large I_o and small Ω. All these features may be understood as follows. Since in all these calculations, the length of the amplifier L is taken to be much smaller than the diffraction length ℓ, the effect due to diffraction and refraction is neglibible; i.e., the beam remains almost parallel to the axis. This was also confirmed from the numerical calculation. For the largest deviation in all the cases considered, a ray starting at $r = 2.0\ w_o$ at the incident plane deflects only to $r = 2.0005\ w_o$ at the output plane. Thus, if one neglects the effect due to diffraction and refraction, Eqs. (3.4), (3.7), (3.8) would reduce to a single equation

$$\frac{dI}{d\zeta} = \frac{g\ell I}{1 + \Omega^2 + I} \qquad (3.9)$$

for an incident collimated beam. This equation is exactly the formula Bridges used in his calculation.[2] As may be seen from Eq. (3.9), the distortion due to saturation is independent of the beam size, w_o, but depends on the detuning Ω and the incident intensity.

IV. UNSTABLE RESONATOR SOLUTIONS

Although the solution of the equations for a wave propagating in an amplifying medium gives some insight into the effects of saturation, detuning, and diffraction on the divergence of the beam, it is necessary to model the amplifying medium in a resonator in order to get a more physically correct picture. Diffraction in particular is likely to assume significance in the case of the resonator due to repeated passes and, specifically in the case of the unstable resonator, the presence of the edges of the output mirror must be taken into account.

The most applicable work done in the past on unstable resonators with an active medium was that of Sziklas and Siegman[5,6] and that of Rensch.[7] Sziklas and Siegman divided the laser into a number of axial segments bounded by transverse stations, where each station has a fixed gain and phase profile. In Ref. 5 they carried out the free-space propagation between stations using Hermite-Gaussian functions as a basis set in an eigenfunction expansion. This required large amounts of computer time for systems with large fresnel numbers, which are of interest in high power lasers. The amount of computer time required is proportional to N^4, where N is the fresnel number. In their later work, Ref. 6, they increased computational efficiency with a discrete Fourier transformation carried out using the fast Fourier transform algorithm. In this approach, computational time increases as $N^2 \log_2 N$, which is smaller for large fresnel numbers, but is still very large if one considers fresnel numbers of 500 to 2000, which are of prime current interest. Rensch used a numerical procedure employing a finite difference method to solve the wave equation. The resonator was

divided into a series of axial segments with each segment considered axially uniform in saturated gain and index of refraction. Propagation through each segment is by an algorithm that satisfies the free-space wave equation. After propagation through a segment, the amplitude and phase of the field are adjusted according to the average gain and index of refraction for that segment. Computational time for this approach is, for a symmetric resonator, $3N^2 \frac{L}{\Delta z}$, where L is the length of the resonator and Δz is the length of the axial segment over which the gain and index is considered uniform. Both of the above methods have a discrete instead of continuous medium in the laser.

The previous method used in the calculation for the beam distortion in an amplifier system is now extended to the calculation of the transverse mode, beam quality, and power-output for an oscillator. For simplicity, the oscillator is again assumed to be circular with axial symmetry, only azimuthally symmetric modes are studied.

An oscillator in general consists of two mirrors, mirror 1 which will be called the output or the front mirror, mirror 2, the back mirror. These two mirrors can be either concave or convex towards to the interior of the cavity with different radii of curvature and can be of different sizes. However, for most high power lasers, the commonly adopted system is usually the positive-branch confocal unstable resonator. In such a system, mirror 1 is a small convex mirror and mirror 2 a concave mirror with much larger size and longer focal length. Figure 19 illustrates such a system. Though the following calculational method is not restricted to such types of resonators, the emphasis throughout is on this type, which is widely used in large laser devices.

The procedure employed for calculating the transverse mode of such resonators is to introduce two planes, plane 1 just in front mirror 1 and plane 2 just in front mirror 2 as shown in Figure 19. To carry out the calculation, an initial left-going wave with its intensity and slope is assumed at plane 1. It propagates to plane 2 using the algorithm described already in detail in the previous section, since propagating from plane 1 to plane 2 is identical to propagating from the input plane to the output plane in an amplifier. After reaching plane 2, it reflects back from mirror 2 to plane 2 and becomes a right-going wave. This wave is propagated to plane 1, again using the same alogithm. After reaching plane 1 and mirror 1 the beam size has been greatly expanded and is now much larger than the mirror size; therefore, this beam splits into two, one the output beam passing mirror 1, the other a beam reflected back to plane 1 which becomes a left-going wave. This calculation can be carried out indefinitely until the wave converges to a steady-state stationary distribution, the resulting distribution being the single transverse mode for the resonator and the output beam passing mirror 1 is the output of the laser.

Presented below are some details of this calculation:

1. In propagating the beam from plane 1 to plane 2 (and from plane 2 back to plane 1), the gain is subject to saturation. This saturation gain, unlike that in an amplifier, is determined by the existing total intensity, i.e., the sum of the left-and right-going intensities at this point. To include both intensities in the gain distribution, the intensities of the on-going wave are stored in memory. These values are added to the opposite traveling wave intensity on the next pass.

Usually, opposite traveling rays do not cross at the same point, in this case, a simple interpolation procedure is required using those stored values from the previous pass of neighboring points.

2. Reflecting from mirror 2: Since mirror 2 is assumed to be larger than the beam size, there will be no edge effect. The field is treated as though it were physically reflected from the surface of the mirror. Its intensity and slope are adjusted for mirror curvature, tilt, and reflectivity. If one assumes that there is no tilt or absorption, to a good approximation, there will be no change in intensity and ray position as the distance between plane 2 and mirror 2 is extremely small. The only change is in the ray slope with

$$v_{refl} = v_{inc} - \frac{2\rho}{R}$$

where v_{inc} and v_{refl} are the slopes of the incident and reflected rays, respectively, ρ is the ray position, R is the radius of curvature of the mirror taken to be positive (negative) for a concave (convex) mirror. The left-going wave now becomes a right-going wave.

3. Reflecting from mirror 1: In addition to a change in ray slopes upon this reflection, mirror 1 is smaller than the size of the now expanded beam, and consequently the beam upon reflection must also be truncated according to the shape of the mirror. At this point, a severe limitation in this numerical technique is apparent. It <u>cannot</u> treat sharp mirror edges. The transverse derivative with respect to ρ is not defined at the mirror edge or at any point the amplitude is discontinuous. To overcome this difficulty, the sharp mirror edge is smoothed out by introducing an effective reflectivity of the mirror

which has a gaussian profile near the mirror edge.

$$R = e^{-(\rho-\rho_o)^2/\tau^2} \qquad \text{for} \quad \rho \geq \rho_o$$

and

$$R = 1 \qquad \text{for} \quad \rho \leq \rho_o$$

where R is the reflectivity of the mirror, ρ_o is the mirror radius within which the reflectivity is uniform, and τ is the truncated distance. For simplicity, it is further assumed that the distance from ρ_o to the physical edge of the mirror is equal to one truncated distance τ. Figure 20 shows schematically how the mirror edge is treated. Two different values τ are shown.

4. After one round trip, the number of rays reflected from mirror surface 1 is greatly reduced as many of them will pass it without being interrupted and those reflected are no longer separated at equal distance. In order to regain the same number of equally separated rays as at the starting point, a simple interpolation procedure is used based on the rays reflected from mirror 1.

5. To begin the calculation, a left-going wave with assumed slopes and intensities is launched from plane 1. The choice of these initial values will make a difference in the amount of computer time needed to yield a stationary solution. A good estimation can be obtained from a simple geometric optics calculation. It is assumed that the left-going wave leaving plane 1 is a spherical wave whose virtual center lies at a point P_1 behind the mirror 1.[8] The intensity is assumed to be a constant intensity I_o multiplied by the effective reflectivity of mirror 1. This constant intensity, I_o can be estimated from the gain of the medium and the output coupling of the system using geometric optics.

A specific computer calculation is made. The system is assumed to be confocal. A complete list of the parameters used for this calculation is listed below:

Radius of curvature of mirror 1	$R_1 = -535$ cm
Radius of curvature of mirror 2	$R_2 = 995$ cm
Length of the cavity	$L = 230$ cm
Radius of mirror 1	$a_1 = 3.2$ cm
Radius of mirror 2	$a_2 = 6.0$ cm
Small signal gain	$g = 0.005$/cm
Frequency shift from gain center	$\Omega = 0.0$
Truncated distance	$\tau = 0.1\ a_1$

An initial spherical wave with $I_o = 0.50\ I_s$, where I_s is the saturation intensity, is launched from plane 1. Fifty-three rays at equal separation, 0.025 a_1, are taken. The number of steps in integration along a ray from one plane to the other is 115. After seven or eight return passes, the solution converges. The total computer time is about three minutes on a UNIVAC 1108 system. Figure 21 shows the intensity and phase at the output plane, the abscissa scale being normalized to a_1. The vertical line at 1 represents the physical edge of mirror 1. The vertical line at 1.86 indicates the beam size at the output plane according to geometric optics (the output coupling for this system based on geometric optics is 71%). Figure 21 shows that the load is almost uniform on mirror 1 and the output intensity increases and then tapers off very quickly near the geometric edge of the beam. The phase is also nearly uniform except near the geometric edge of the beam. Figure 22 shows the normalized far-field distribution calculated using the

intensity and phase of the output beam at the near-field. The far-field distribution shown in Figure 22 is very nearly identical to a diffraction limited distribution and has a first side-lobe peak intensity equal to approximately 10% of the main lobe. The peak intensity at $\theta = 0$, when focussed at one diffraction length, ka_1^2, is found to be 1.21 I_s. The dashed curve in Figure 22 is the integrated power normalized to the total power (energy in the "bucket"). As shown, more than 80% of the power is within an angle $\theta = \frac{\lambda}{2a_1}$ and more than 90% of the power within $\theta = 1.5 \times \frac{\lambda}{2a_1}$. The total output power is found to be 49.9 I_s watts when I_s is measured in watts/cm^2.

Figures 23 and 24 show an identical calculation, but this time with $\Omega = 0.2$. The result of this calculation is almost identical to that with $\Omega = 0.0$, except the output power is reduced by a small percentage. The peak intensity at far-field is now 1.14 I_s and the total output power is reduced to 47.1 I_s watts. This calculation indicates that the effect due to detuning of the driving frequency from the gain center is not important as expected.

Figures 25 and 26 are the result of a calculation with the small signal gain, g, reduced to 0.004/cm. As expected, the output power is greatly reduced. The peak intensity at far-field is now 0.63 I_s and the total output power is 26.5 I_s watts. The intensity and phase distributions at near-field and far-field remain unchanged.

Lastly, the effect due to mirror edge is tested. A different truncated distance $\tau = 0.05\ a_1$ is used. A smaller τ corresponds to a sharper mirror edge and is closer to physical reality. Figures 27 and 28 are the result of this calculation. It is seen that the intensity

and phase distributions at the near-field remain almost exactly the same as before except near the geometric edge of the beam where they fluctuate more. The far-field pattern is also almost identical, the beam being slightly more divergent. The total output power remains the same, but the peak intensity is down to 1.07 I_s with the result that the power is down about 10% in the same "bucket."

V. CONCLUSIONS AND RECOMMENDATIONS

Laser media of the general characteristics of the CW-EDL when considered as an amplifier driven at a moderate fraction of the saturation intensity show little beam distortion for a gaussian input beam. There are only small saturation effects, and very little effect for detuning of the driving frequency from the center of the gain line. For beams, such as those considered here, which have diameters of many times the propagating wavelength, diffraction due to the finite beam size is negligible.

When the system is modelled as an oscillator, assuming cylindrical geometry, diffraction effects appear, causing a departure in phase and intensity from the uniform phase and intensity to be expected on solely geometric considerations. These departures from the uniform plane wave cause, in turn, a change in the far-field intensity pattern. While this azimuthally symmetric model approximation yields some valuable insight into system behavior and is of great value in establishing model and calculation procedure validity, a model in rectangular coordinates providing for variation in the gain media in both the transverse directions would surely be more accurate.

One observation that might be made is that the far-field intensity pattern might be improved by increasing the system feedback, as the medium could be driven harder. This could be accomplished by increasing the diameter of the output mirror, and making other necessary related changes. Otherwise, there seems no advantage in changing the resonator geometry.

It is recommended that further study be carried out on this system using the theories and procedures developed here. Specifically, the system should be set up in rectangular coordinates with the variations of the media in the transverse directions included in the calculations. The effect of variation in feedback on the far-field intensity should be studied on the computer, as it is relatively complex, interacting as it does with the medium saturation and the output aperture size.

REFERENCES

1. M. Lax, W. H. Louiselll and W. B. McKnight, Phys. Rev. A11, 989 (1975).

2. W. B. Bridges, IEEE Jour. Quan. Elec. QE-4, 820 (1968).

3. W. G. Wagner, H. A. Haus, and J. H. Marburger, Phys. Rev. 175, 256 (1968); V. I. Talanov, Zh. Eksp. Teor. Fiz. Pis'ma Red. 2, 218 (1965) [JETP Lett. 2, 138 (1965)]; Yu. P. Raiser, Zh. Edsp. Teor. Fiz. Pis'ma Red. [JETP Lett. 4, 1 (1966)]; H. Kogelnik, Appl. Opt. 4, 1562 (1965); P. L. Kelley, Phys. Rev. Lett. 15, 1005 (1965).

4. H. Kogelnik and T. Li, Proc. IEEE, 54 1312 (1966); G. D. Boyd and J. P. Gordon, Bell Syst. Tech. J. 40, 489 (1961); L. A. Vainshtein, Zh. Tekhn. Fiz. 34, 183 (1964).

5. A. E. Siegman and E. A. Sziklas, Appl. Opt. 13, 2775 (1974).

6. E. A. Sziklas and A. E. Siegman, Appl. Opt. 14, 1874 (1975).

7. D. B. Rensch, Appl. Opt. 13, 2546 (1974).

8. A. E. Siegman, Proceedings of IEEE 53, 277 (1965).

Input Parameters			Peak Intensity at Output Plane in Units of I_S		
w_o in cm	I_o in I_S	Ω	L = 100 cm	L = 200 cm	L = 400 cm
2.5	0.1	0.0	0.237	0.497	1.436
2.5	0.1	0.1	0.235	0.492	1.419
2.5	0.1	0.5	0.205	0.392	1.098
2.5	0.25	0.0	0.519	0.933	2.115
2.5	0.25	0.1	0.517	0.927	2.099
2.5	0.25	0.5	0.467	0.798	1.782
2.5	0.5	0.0	0.906	1.442	2.783
2.5	0.5	0.1	0.903	1.435	2.768
2.5	0.5	0.5	0.844	1.301	2.480
5.0	0.1	0.0	0.237	0.497	1.436
5.0	0.1	0.1	0.235	0.492	1.420
5.0	0.1	0.5	0.205	0.392	1.101
5.0	0.25	0.0	0.519	0.933	2.115
5.0	0.25	0.1	0.517	0.927	2.100
5.0	0.25	0.5	0.468	0.798	1.788
5.0	0.5	0.0	0.906	1.441	2.784
5.0	0.5	0.1	0.903	1.435	2.771
5.0	0.5	0.5	0.845	1.303	2.490

TABLE I Peak intensity of the output beam at various distances from the input plane, with various input parameters.

FIGURE CAPTIONS

Fig. 1. The spreading on a gaussian input beam at various distances from the input plane. The output peak intensity has been normalized to one. Input parameters are $w_o = 2.5$ cm, $I_o = 0.1\ I_S$, $\Omega = 0.0$.

Fig. 2. Same as Fig. 1, but with $w_o = 2.5$ cm, $I_o = 0.1\ I_S$, $\Omega = 0.1$.

Fig. 3. Same as Fig. 1, but with $w_o = 2.5$ cm, $I_o = 0.1\ I_S$, $\Omega = 0.5$.

Fig. 4. Same as Fig. 1, but with $w_o = 2.5$ cm, $I_o = 0.25\ I_S$, $\Omega = 0.0$.

Fig. 5. Same as Fig. 1, but with $w_o = 2.5$ cm, $I_o = 0.25\ I_S$, $\Omega = 0.1$.

Fig. 6. Same as Fig. 1, but with $w_o = 2.5$ cm, $I_o = 0.25\ I_S$, $\Omega = 0.5$.

Fig. 7. Same as Fig. 1, but with $w_o = 2.5$ cm, $I_o = 0.5\ I_S$, $\Omega = 0.0$.

Fig. 8. Same as Fig. 1, but with $w_o = 2.5$ cm, $I_o = 0.5\ I_S$, $\Omega = 0.1$.

Fig. 9. Same as Fig. 1, but with $w_o = 2.5$ cm, $I_o = 0.5\ I_S$, $\Omega = 0.5$.

Fig. 10. Same as Fig. 1, but with $w_o = 5.0$ cm, $I_o = 0.1\ I_S$, $\Omega = 0.0$.

Fig. 11. Same as Fig. 1, but with $w_o = 5.0$ cm, $I_o = 0.1\ I_S$, $\Omega = 0.1$.

Fig. 12. Same as Fig. 1, but with $w_o = 5.0$ cm, $I_o = 0.1\ I_S$, $\Omega = 0.5$.

Fig. 13. Same as Fig. 1, but with $w_o = 5.0$ cm, $I_o = 0.25\ I_S$, $\Omega = 0.0$.

Fig. 14. Same as Fig. 1, but with $w_o = 5.0$ cm, $I_o = 0.25\ I_S$, $\Omega = 0.1$.

Fig. 15. Same as Fig. 1, but with $w_o = 5.0$ cm, $I_o = 0.25\ I_S$, $\Omega = 0.5$.

Fig. 16. Same as Fig. 1, but with $w_o = 5.0$ cm, $I_o = 0.5\ I_S$, $\Omega = 0.0$.

Fig. 17. Same as Fig. 1, but with $w_o = 5.0$ cm, $I_o = 0.5\ I_S$, $\Omega = 0.1$.

Fig. 18. Same as Fig. 1, but with $w_o = 5.0$ cm, $I_o = 0.5\ I_S$, $\Omega = 0.5$.

Fig. 19. The unstable resonator, a_1 is the radius of mirror 1, a_2, the radius of mirror 2, L is the length of the cavity. Planes 1 and 2 are just in front of mirrors 1 and 2, respectively.

Fig. 20. Mirror edge tapering, τ is the truncated distance as defined in the text.

Fig. 21. The near-field intensity and phase at the output plane, the solid curve is for the intensity, dashed curve is for the phase. The vertical line at 1 represents the physical edge of mirror 1. The vertical line at 1.86 represents the beam size according to geometric optics. Input parameters are $g = 0.005/\text{cm}$, $\Omega = 0.0$, $\tau = 0.1\ a_1$.

Fig. 22. The far-field normalized intensity and the energy in the "bucket." Input parameters are $g = 0.005/\text{cm}$, $\Omega = 0.0$, $\tau = 0.1\ a_1$.

Fig. 23. Same as Fig. 21, but with $g = 0.005/\text{cm}$, $\Omega = 0.2$, $\tau = 0.1\ a_1$.

Fig. 24. Same as Fig. 22, but with $g = 0.005/\text{cm}$, $\Omega = 0.2$, $\tau = 0.1\ a_1$.

Fig. 25. Same as Fig. 21, but with $g = 0.004/\text{cm}$, $\Omega = 0.0$, $\tau = 0.1\ a_1$.

Fig. 26. Same as Fig. 22, but with $g = 0.004/\text{cm}$, $\Omega = 0.0$, $\tau = 0.1\ a_1$.

Fig. 27. Same as Fig. 21, but with $g = 0.005/\text{cm}$, $\Omega = 0.0$, $\tau = 0.05\ a_1$.

Fig. 28. Same as Fig. 22, but with $g = 0.005/\text{cm}$, $\Omega = 0.0$, $\tau = 0.05\ a_1$.

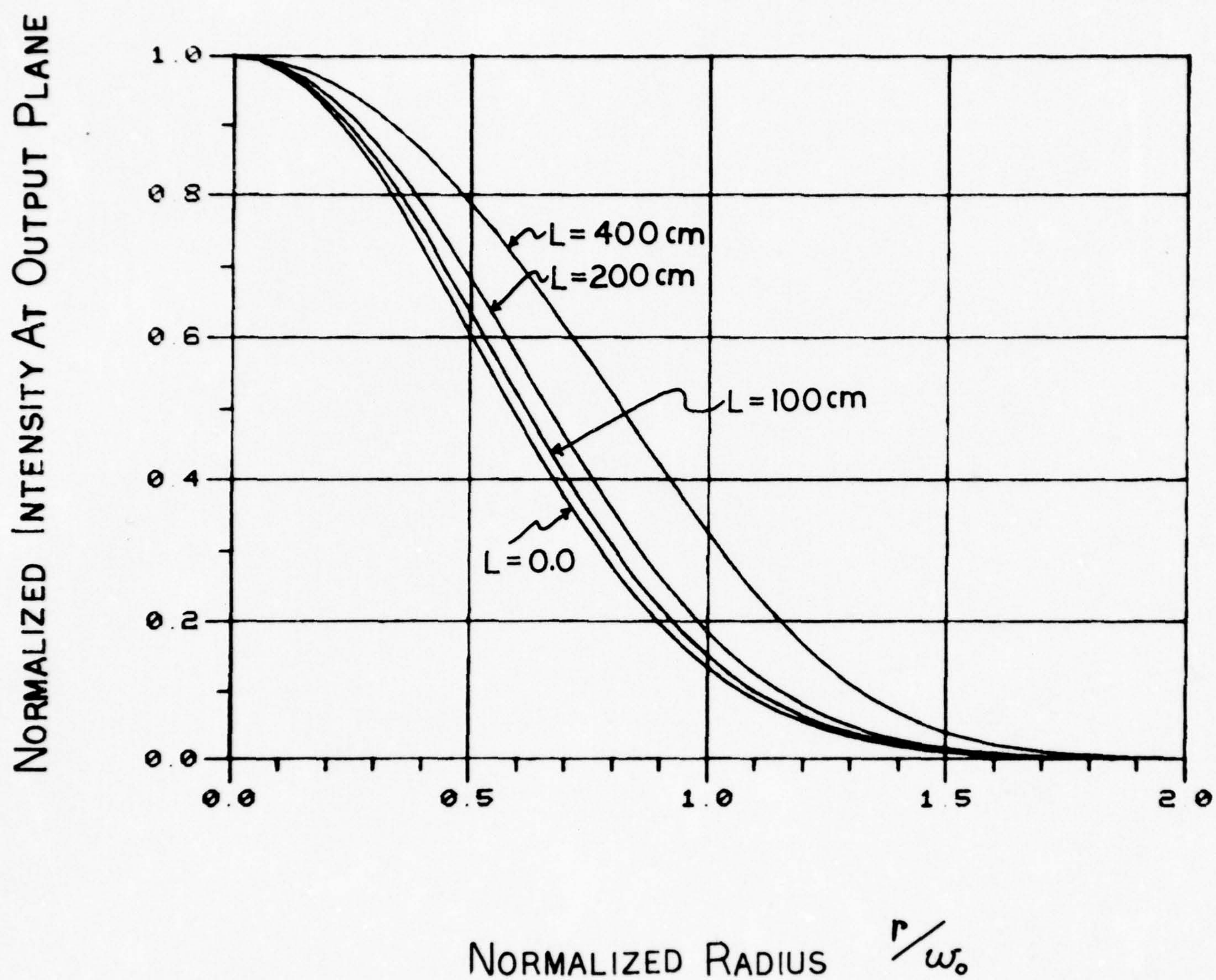

1.0
0.8
0.6
0.4
0.2
0.0
0.0
0.5
1.0
1.5
2.0
L = 400 cm
L = 200 cm
L = 100 cm
L = 0.0
Normalized Intensity At Output Plane
Normalized Radius r/w₀

FIG. 1

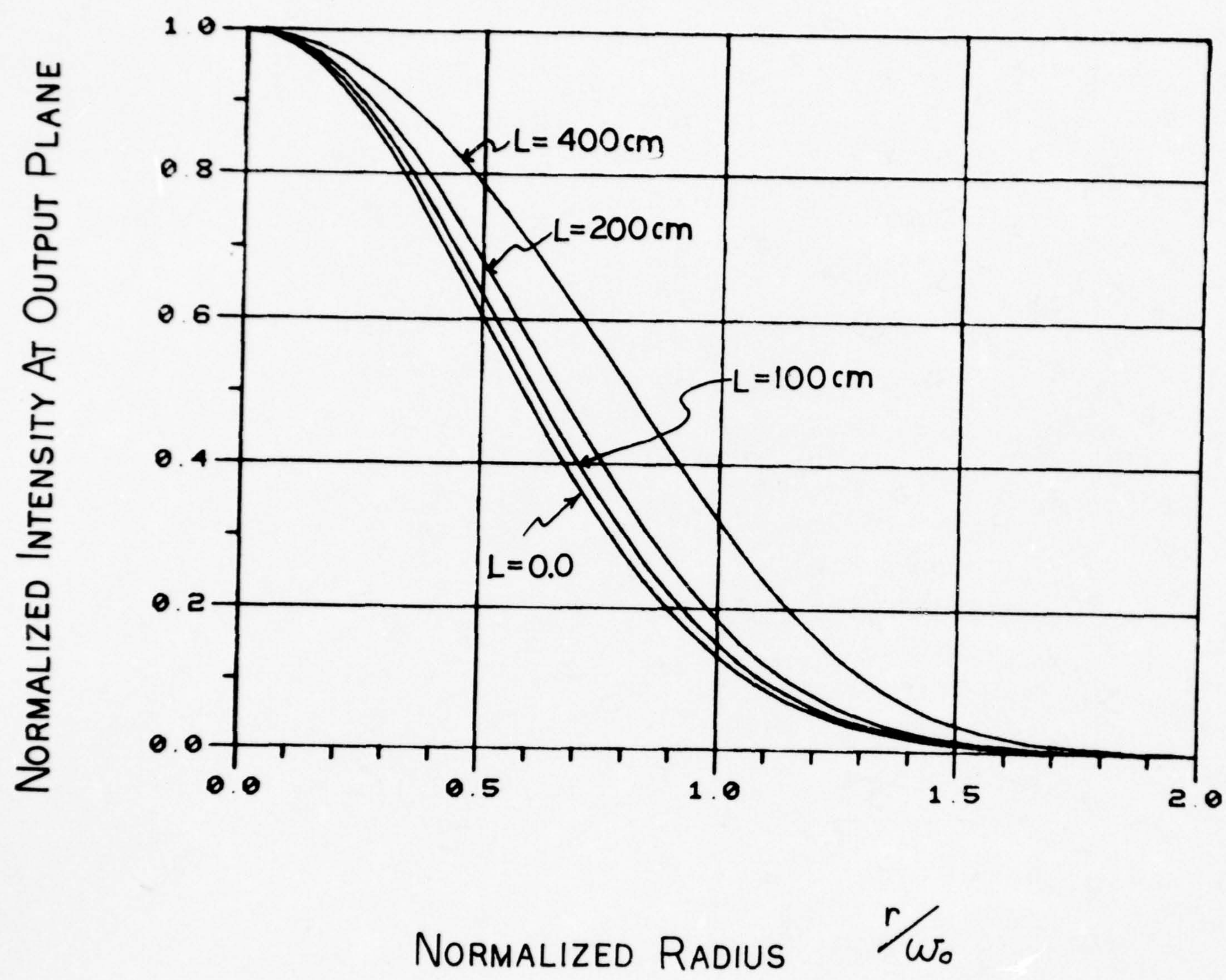
NORMALIZED INTENSITY AT OUTPUT PLANE
1.0
0.8
0.6
0.4
0.2
0.0
0.0
0.5
1.0
1.5
2.0
L=400cm
L=200cm
L=100cm
L=0.0
NORMALIZED RADIUS r/ω_o

FIG. 2

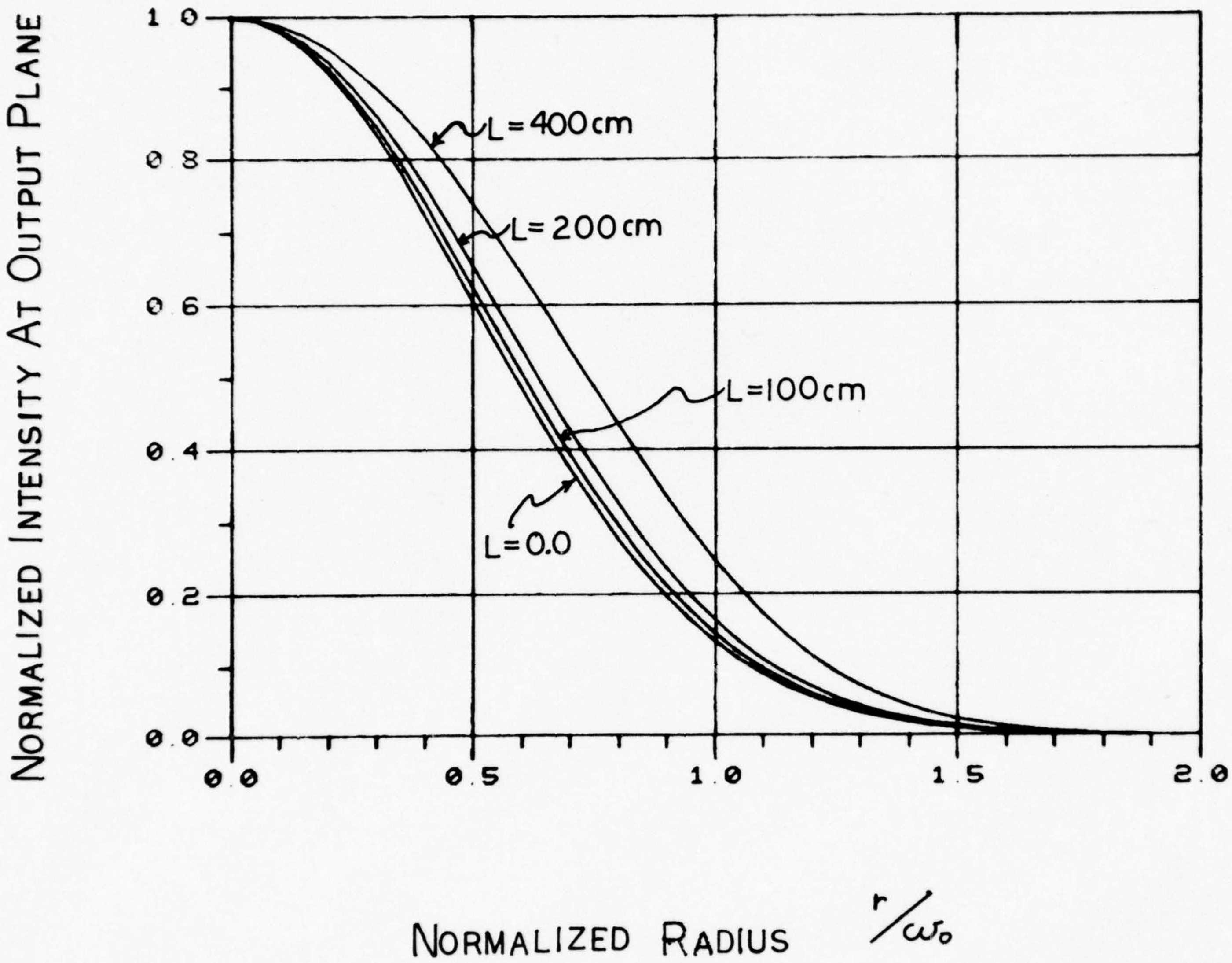

NORMALIZED INTENSITY AT OUTPUT PLANE
1.0
0.8
0.6
0.4
0.2
0.0
0.0
0.5
1.0
1.5
2.0
L=400cm
L=200cm
L=100cm
L=0.0
NORMALIZED RADIUS r/ω₀

FIG. 3

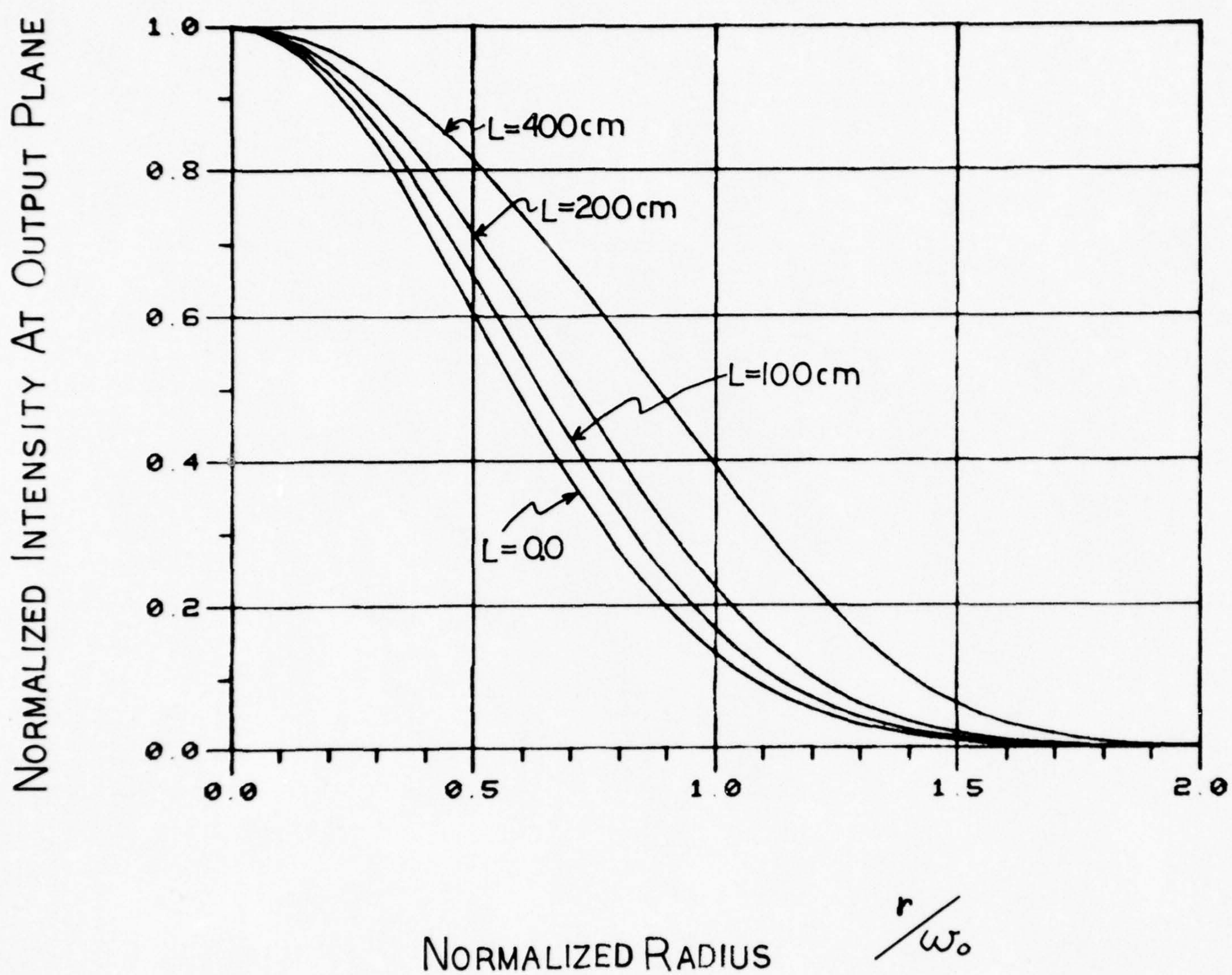
NORMALIZED INTENSITY AT OUTPUT PLANE
1.0
0.8
0.6
0.4
0.2
0.0
0.0
0.5
1.0
1.5
2.0
L=400cm
L=200cm
L=100cm
L=0.0
NORMALIZED RADIUS
r/ω₀

FIG. 4

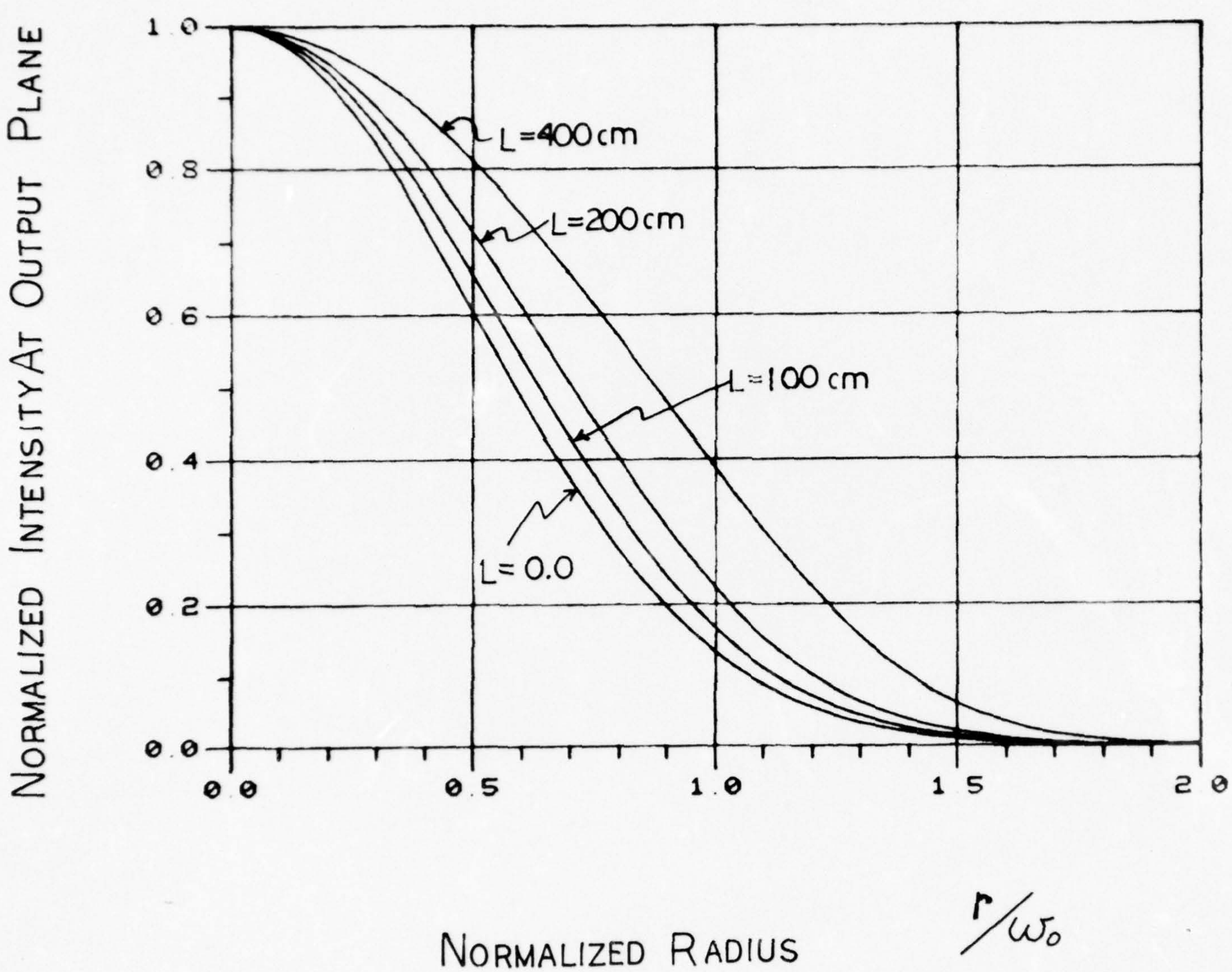
NORMALIZED INTENSITY AT OUTPUT PLANE
1.0
0.8
0.6
0.4
0.2
0.0
0.0
0.5
1.0
1.5
2.0
L=400cm
L=200cm
L=100 cm
L=0.0
NORMALIZED RADIUS
r/ω₀

FIG. 5

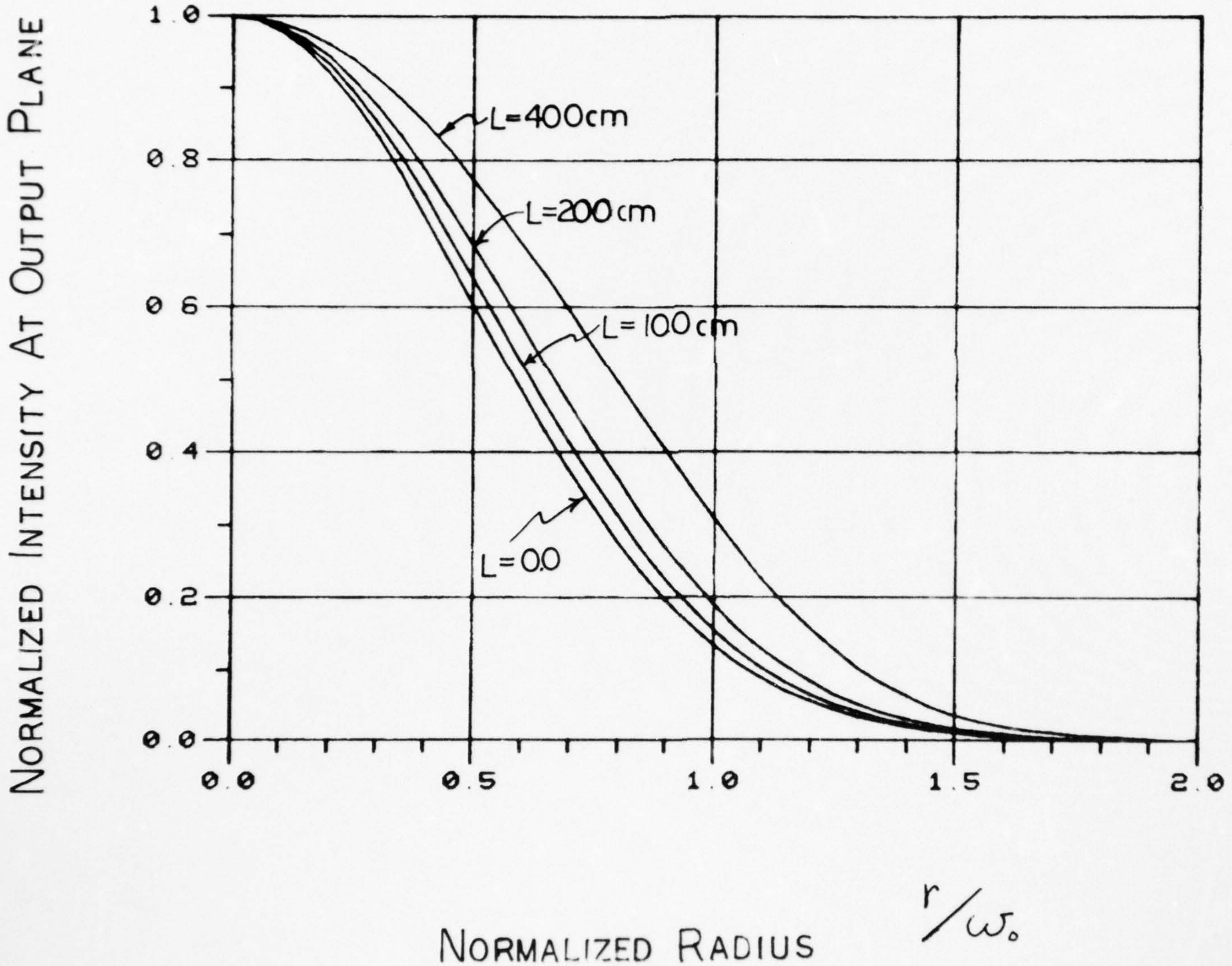

Normalized Intensity At Output Plane
1.0
0.8
0.6
0.4
0.2
0.0
0.0
0.5
1.0
1.5
2.0
L=400cm
L=200cm
L=100cm
L=0.0
Normalized Radius
r/ω₀

Fig. 6

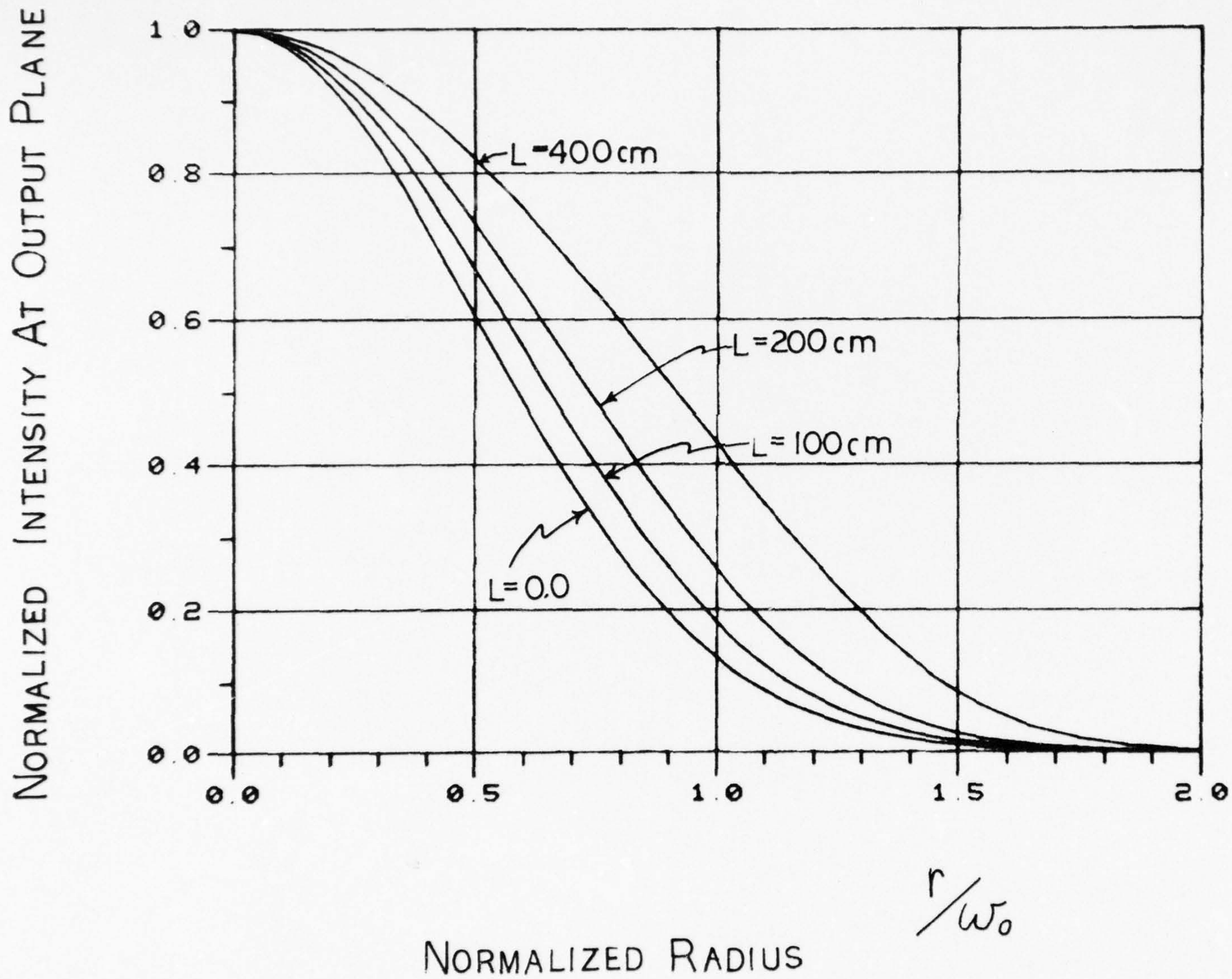
NORMALIZED INTENSITY AT OUTPUT PLANE
1.0
0.8
0.6
0.4
0.2
0.0
0.0
0.5
1.0
1.5
2.0
L=400 cm
L=200 cm
L=100 cm
L=0.0
r/ω₀
NORMALIZED RADIUS

FIG. 7

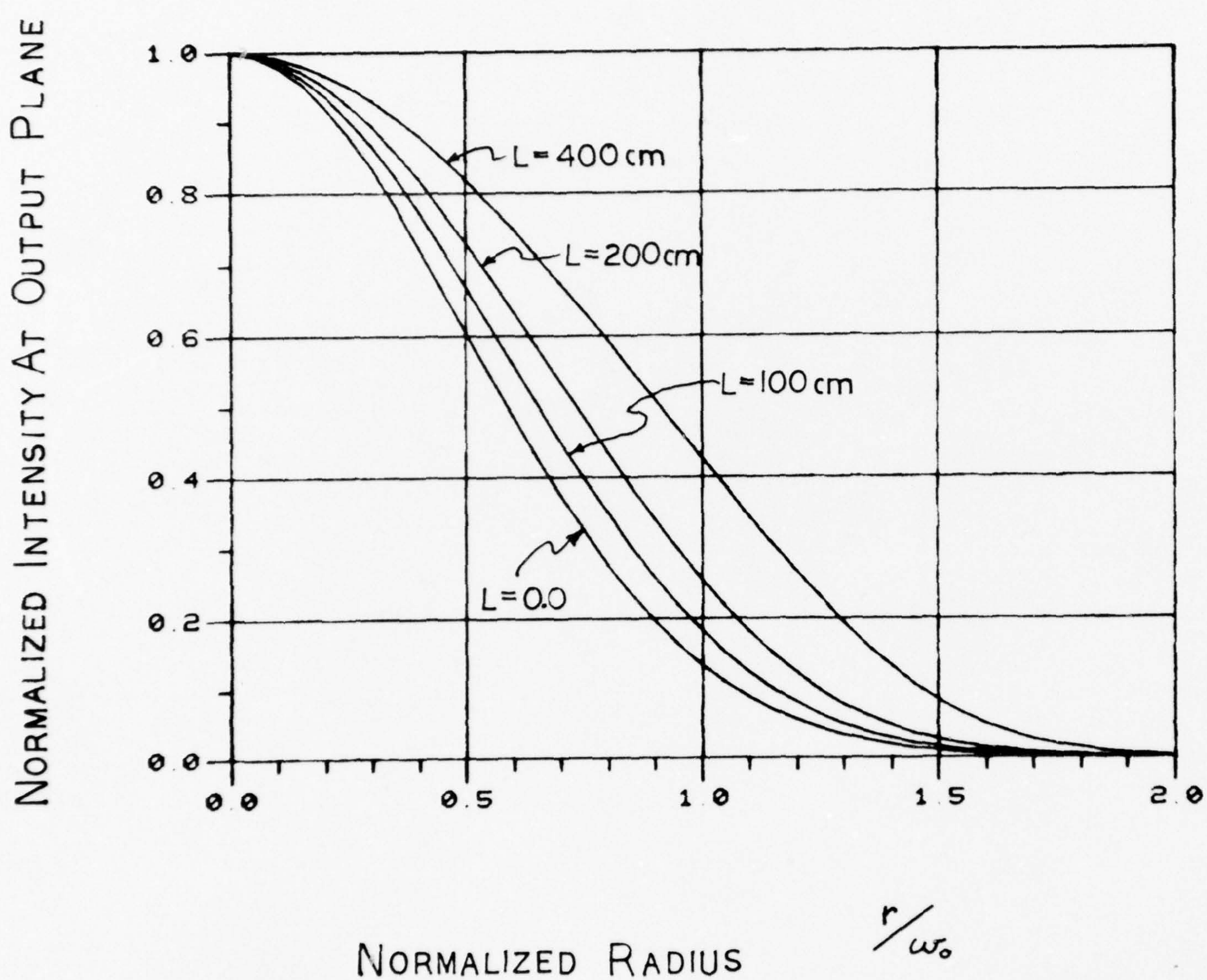

Normalized Intensity At Output Plane
1.0
0.8
0.6
0.4
0.2
0.0
L=400 cm
L=200cm
L=100 cm
L=0.0
0.0
0.5
1.0
1.5
2.0
Normalized Radius
r/ω₀

Fig. 8

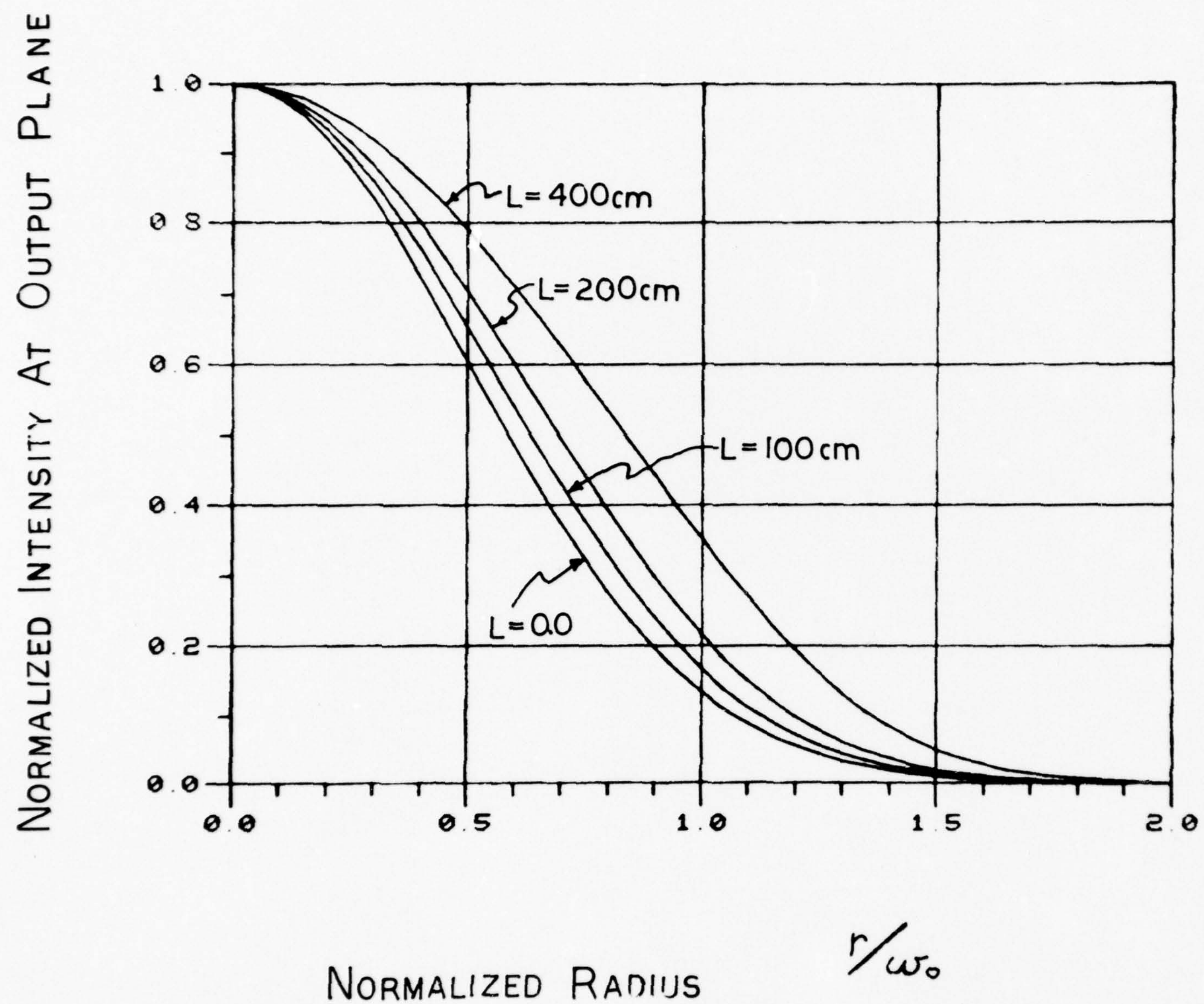
NORMALIZED INTENSITY AT OUTPUT PLANE
1.0
0.8
0.6
0.4
0.2
0.0
0.0
0.5
1.0
1.5
2.0
L=400cm
L=200cm
L=100cm
L=0.0
NORMALIZED RADIUS
r/ω₀

FIG. 9

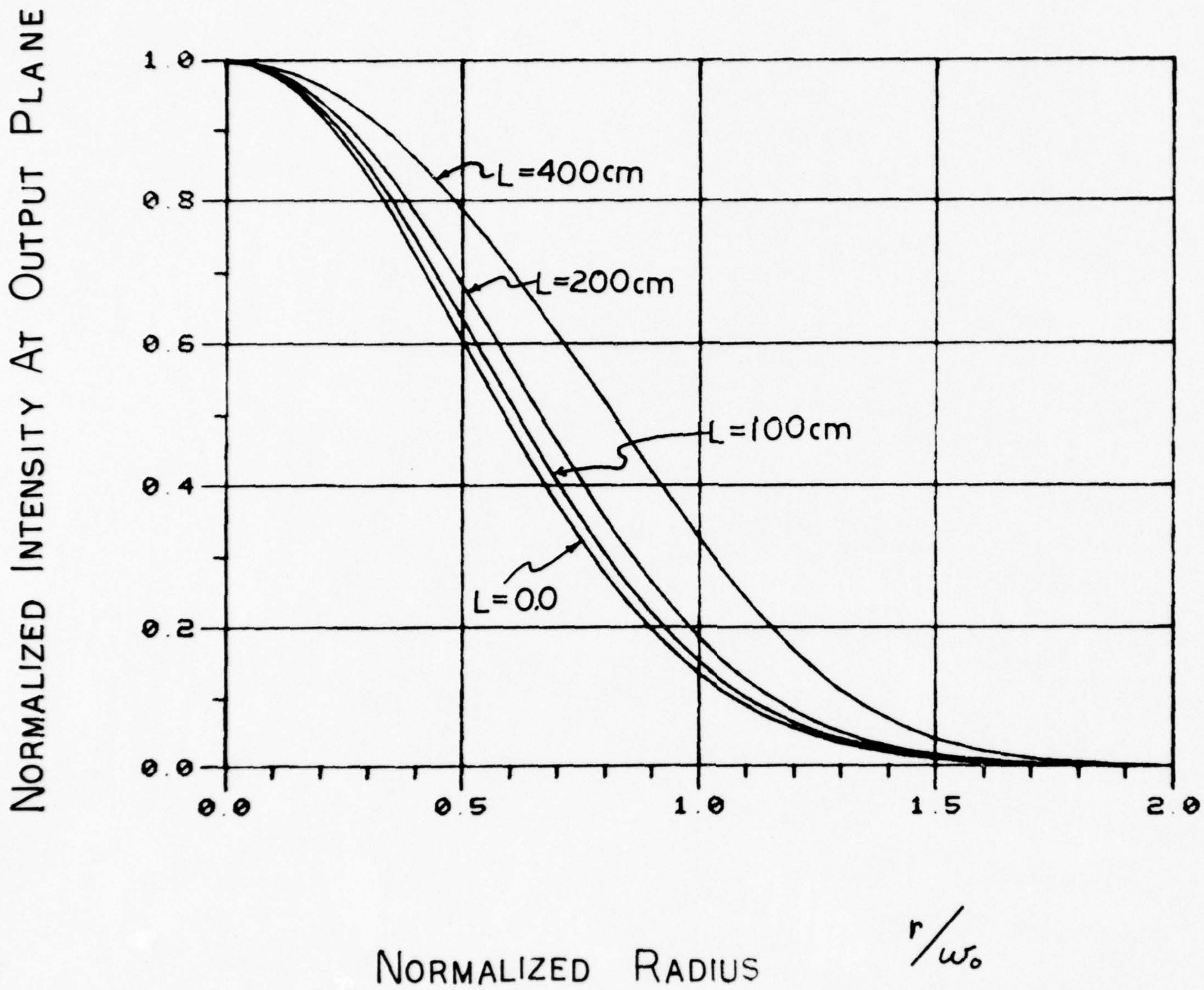

Normalized Intensity At Output Plane
1.0
0.8
0.6
0.4
0.2
0.0
L=400cm
L=200cm
L=100cm
L=0.0
0.0
0.5
1.0
1.5
2.0
Normalized Radius r/w₀

Fig. 10

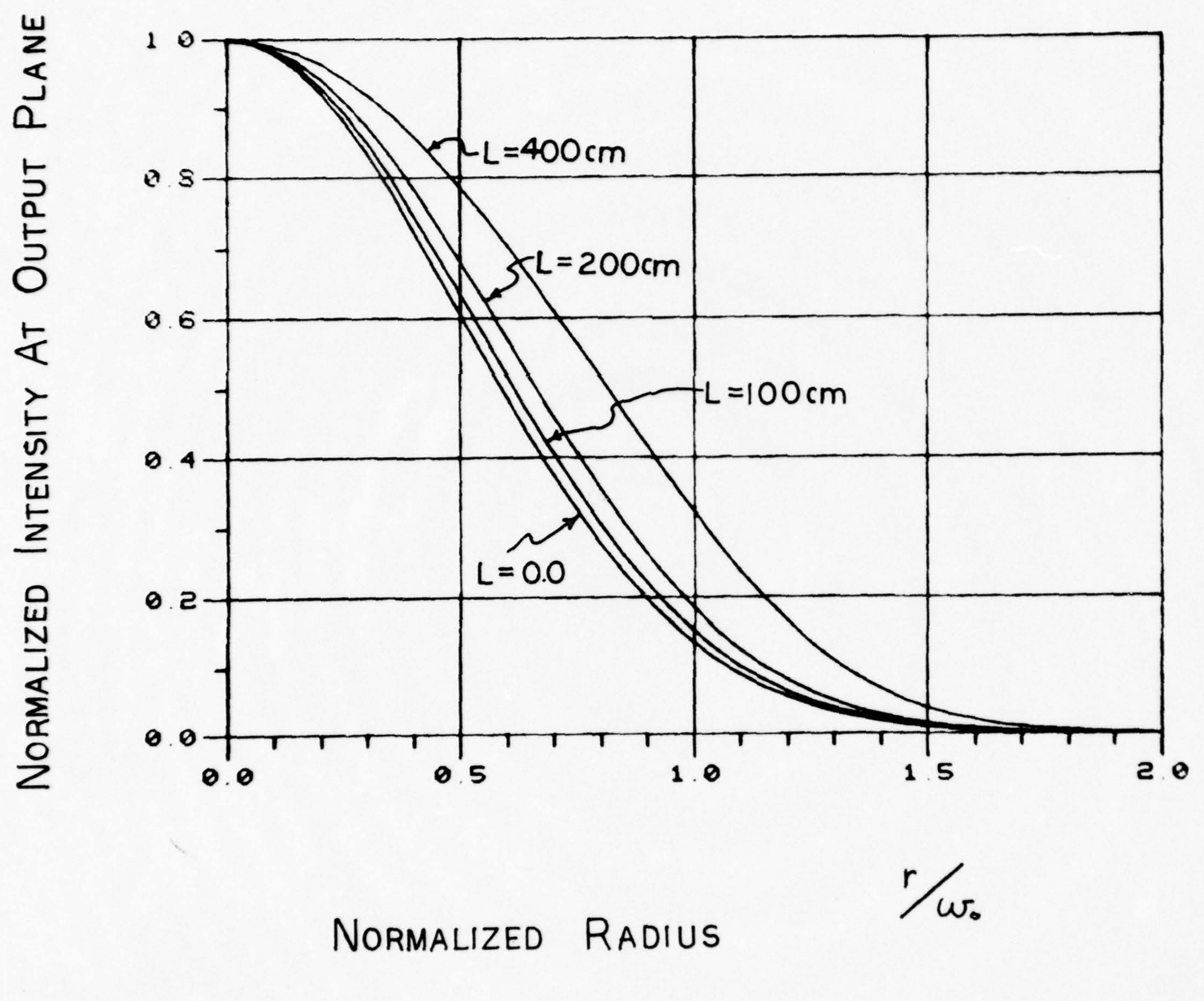

Normalized Intensity At Output Plane
1.0
0.8
0.6
0.4
0.2
0.0
0.0
0.5
1.0
1.5
2.0
L=400cm
L=200cm
L=100cm
L=0.0
r/ω₀
Normalized Radius

Fig. 11

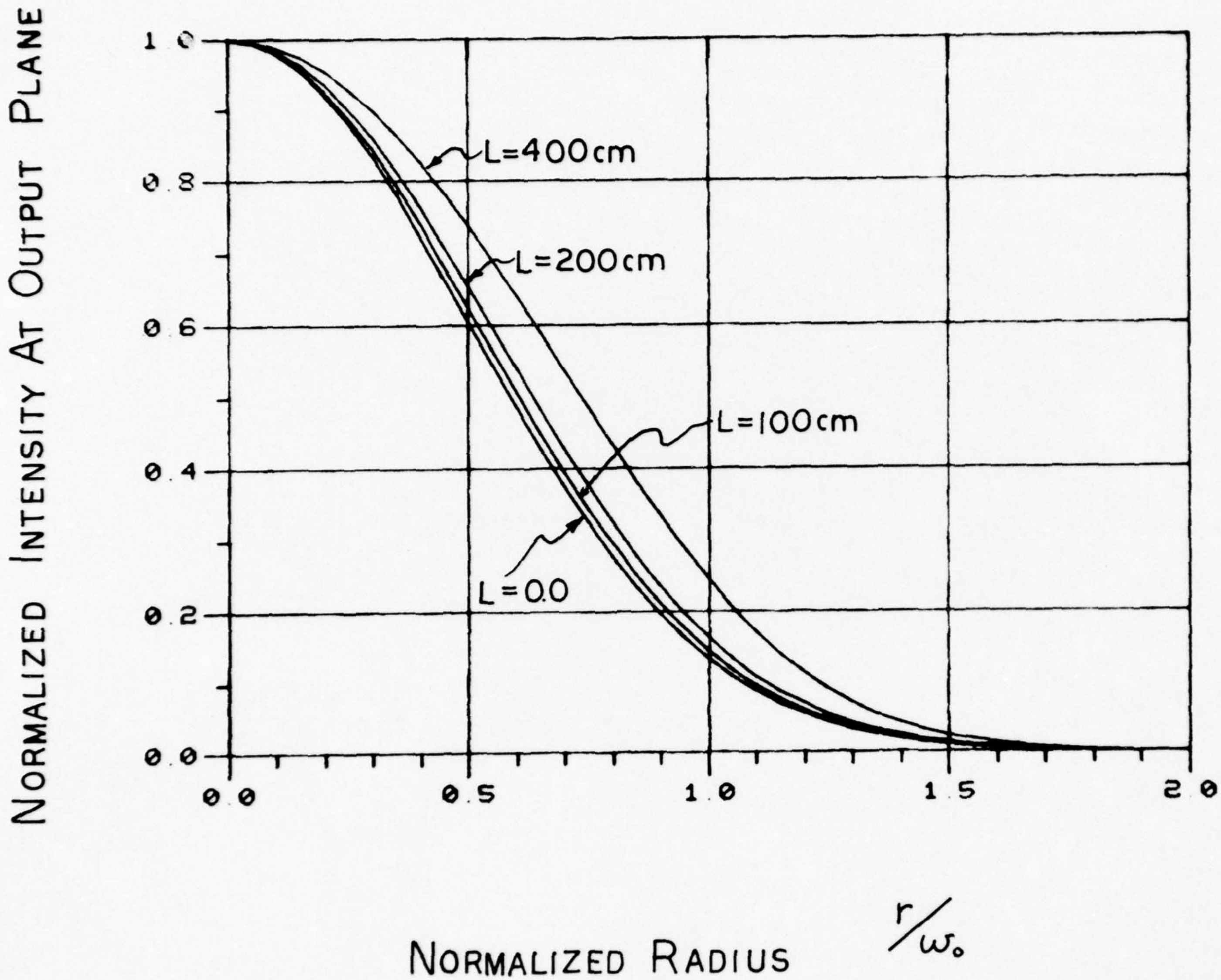

Normalized Intensity At Output Plane
1.0
0.8
0.6
0.4
0.2
0.0
0.0
0.5
1.0
1.5
2.0
L=400cm
L=200cm
L=100cm
L=0.0
Normalized Radius r/ω₀

Fig. 12

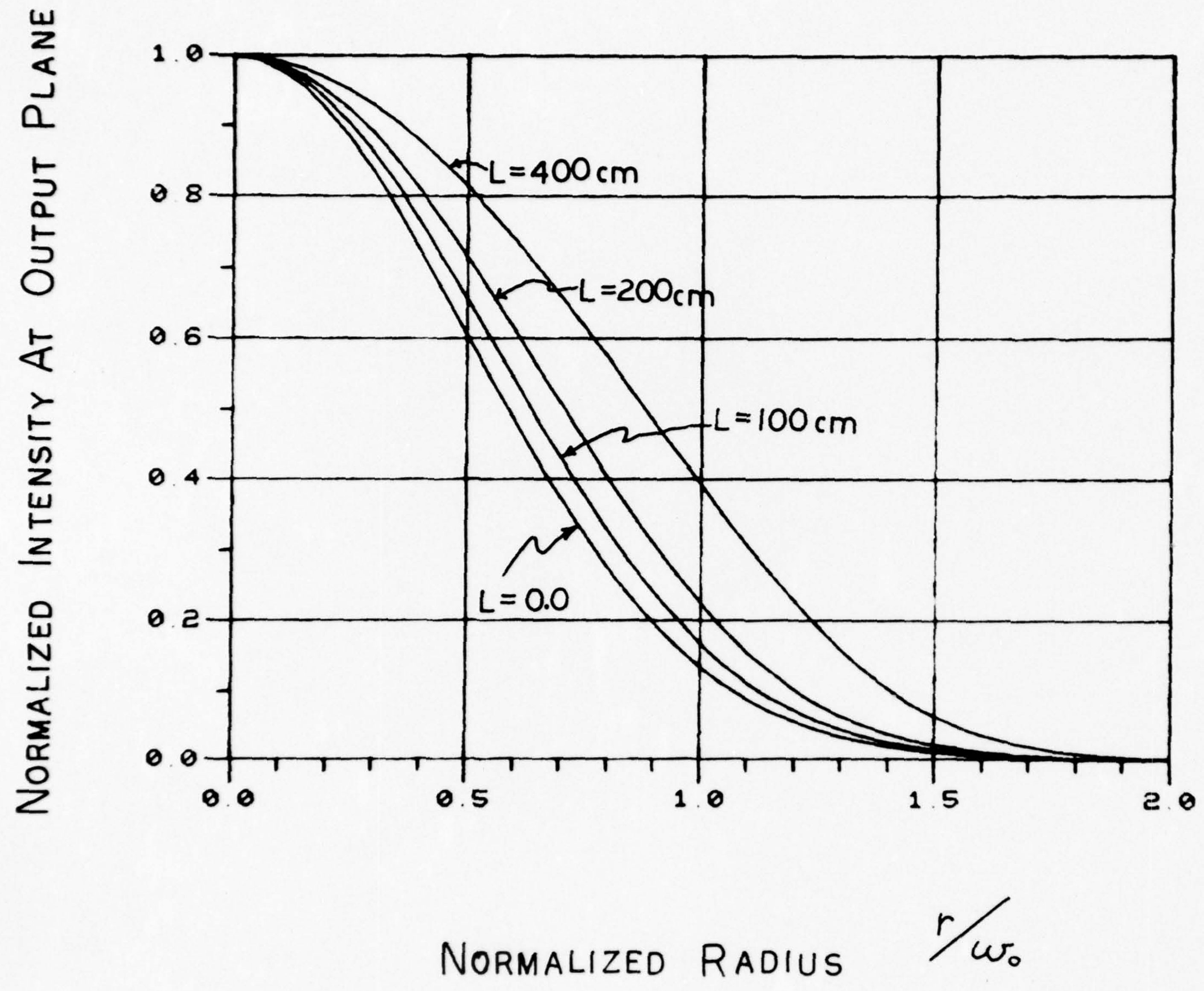

NORMALIZED INTENSITY AT OUTPUT PLANE
1.0
0.8
0.6
0.4
0.2
0.0
0.0
0.5
1.0
1.5
2.0
L=400 cm
L=200cm
L=100 cm
L=0.0
NORMALIZED RADIUS r/ω₀

FIG. 13

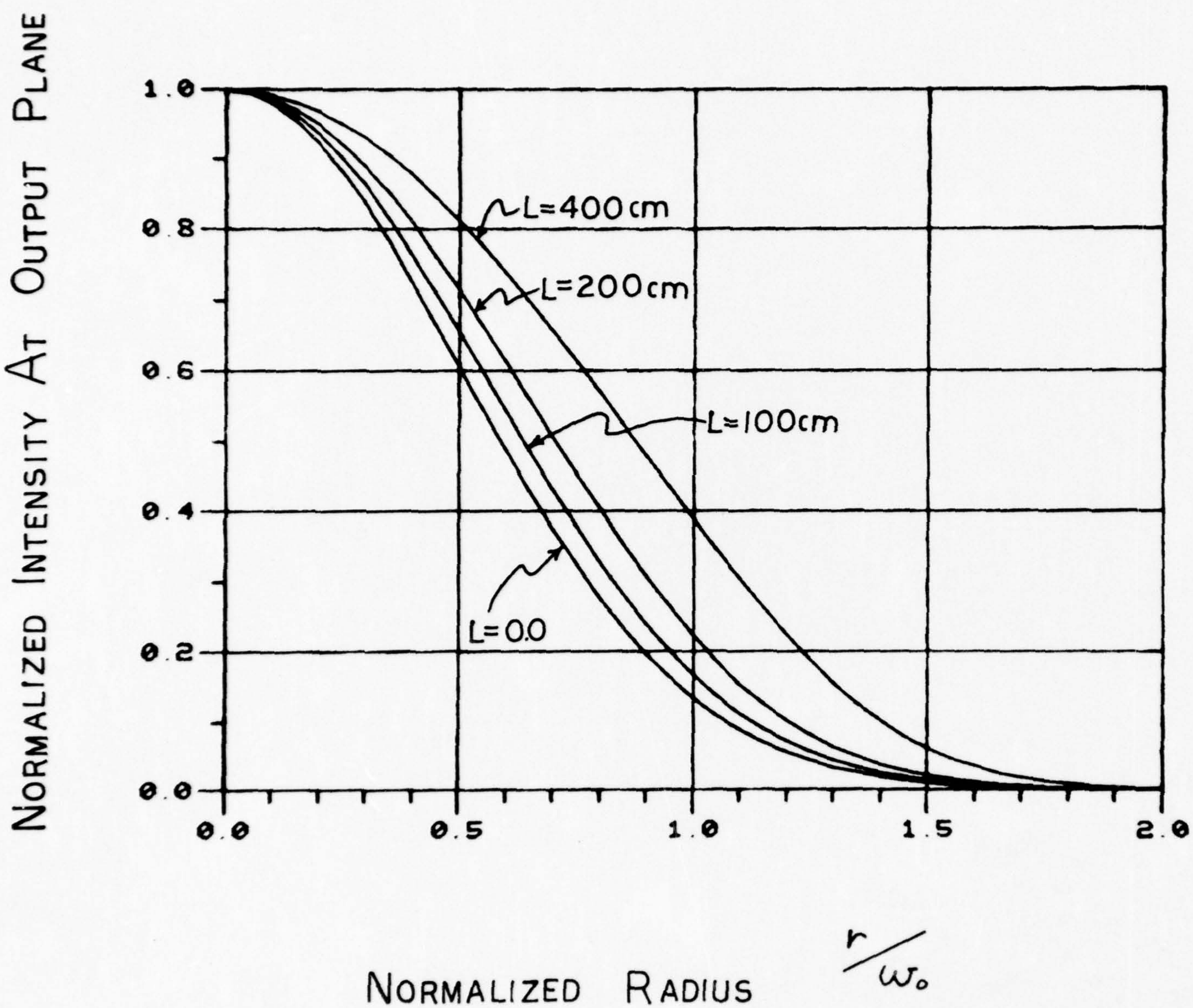

Normalized Intensity At Output Plane
1.0
0.8
0.6
0.4
0.2
0.0
0.0
0.5
1.0
1.5
2.0
L=400cm
L=200cm
L=100cm
L=0.0
Normalized Radius r/ω_o

Fig. 14

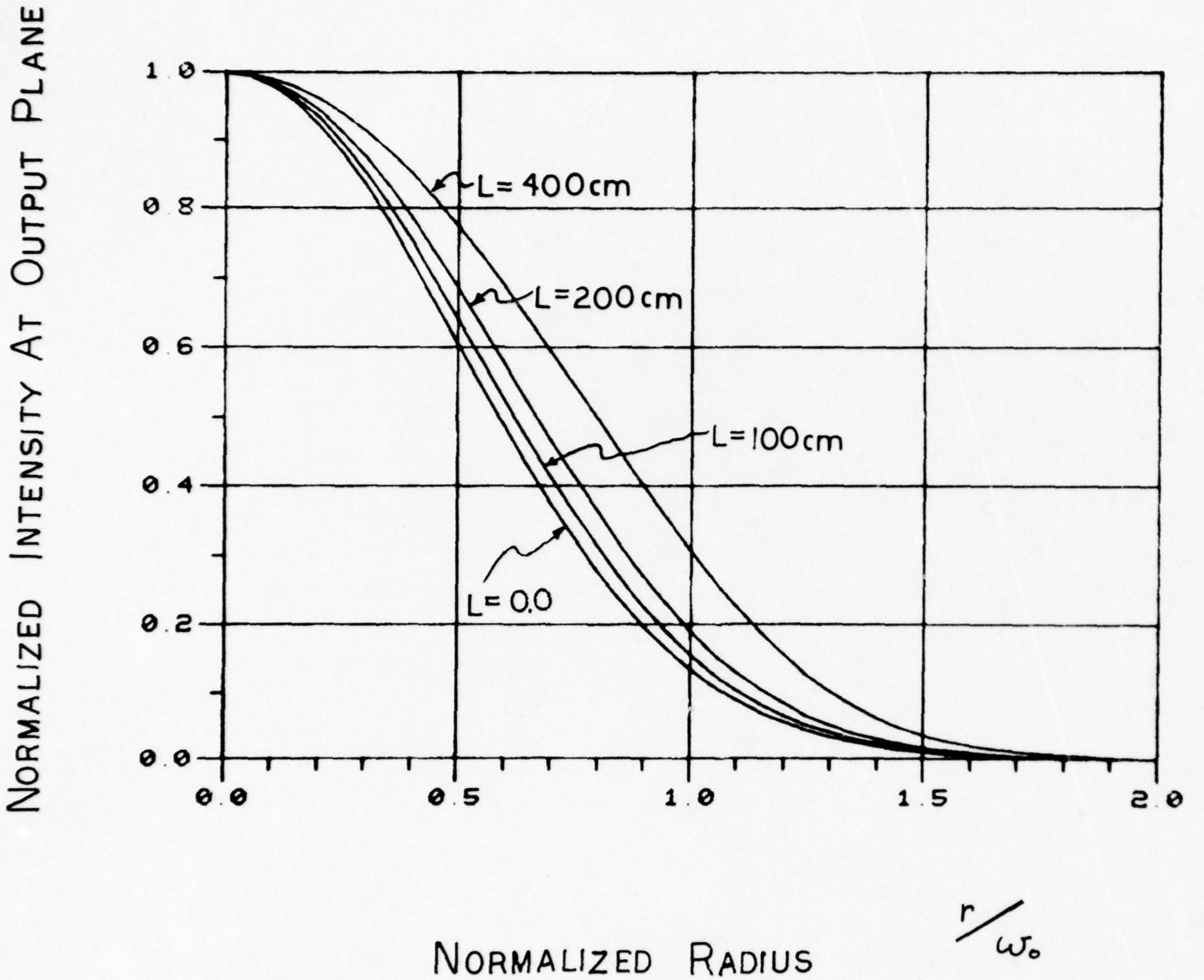

Normalized Intensity At Output Plane
1.0
0.8
0.6
0.4
0.2
0.0
0.0
0.5
1.0
1.5
2.0
L= 400cm
L=200cm
L=100cm
L= 0.0
Normalized Radius
r/ω₀

Fig. 15

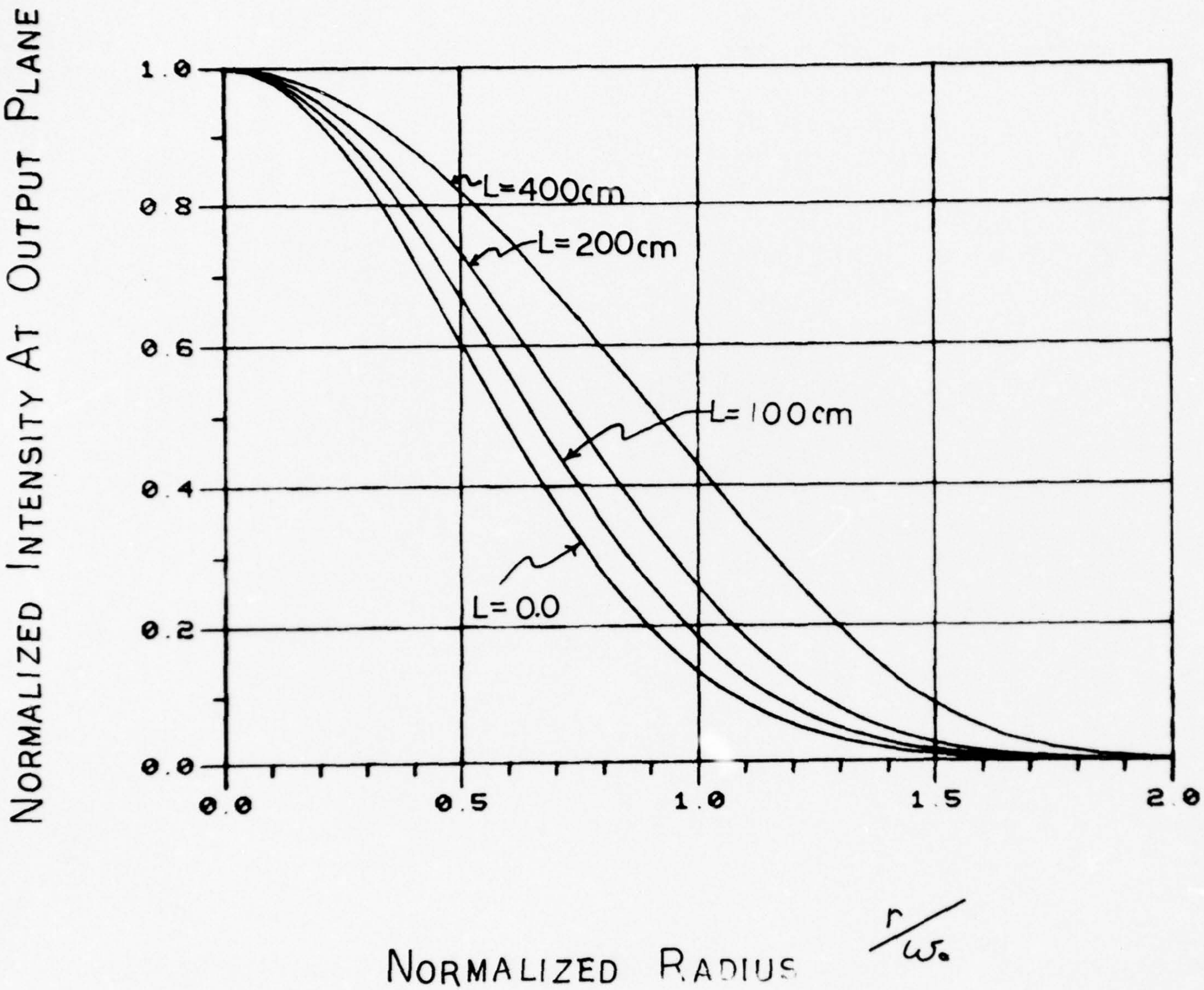
NORMALIZED INTENSITY AT OUTPUT PLANE
1.0
0.8
0.6
0.4
0.2
0.0
0.0
0.5
1.0
1.5
2.0
L=400cm
L=200cm
L=100cm
L=0.0
NORMALIZED RADIUS r/ω₀

FIG. 16

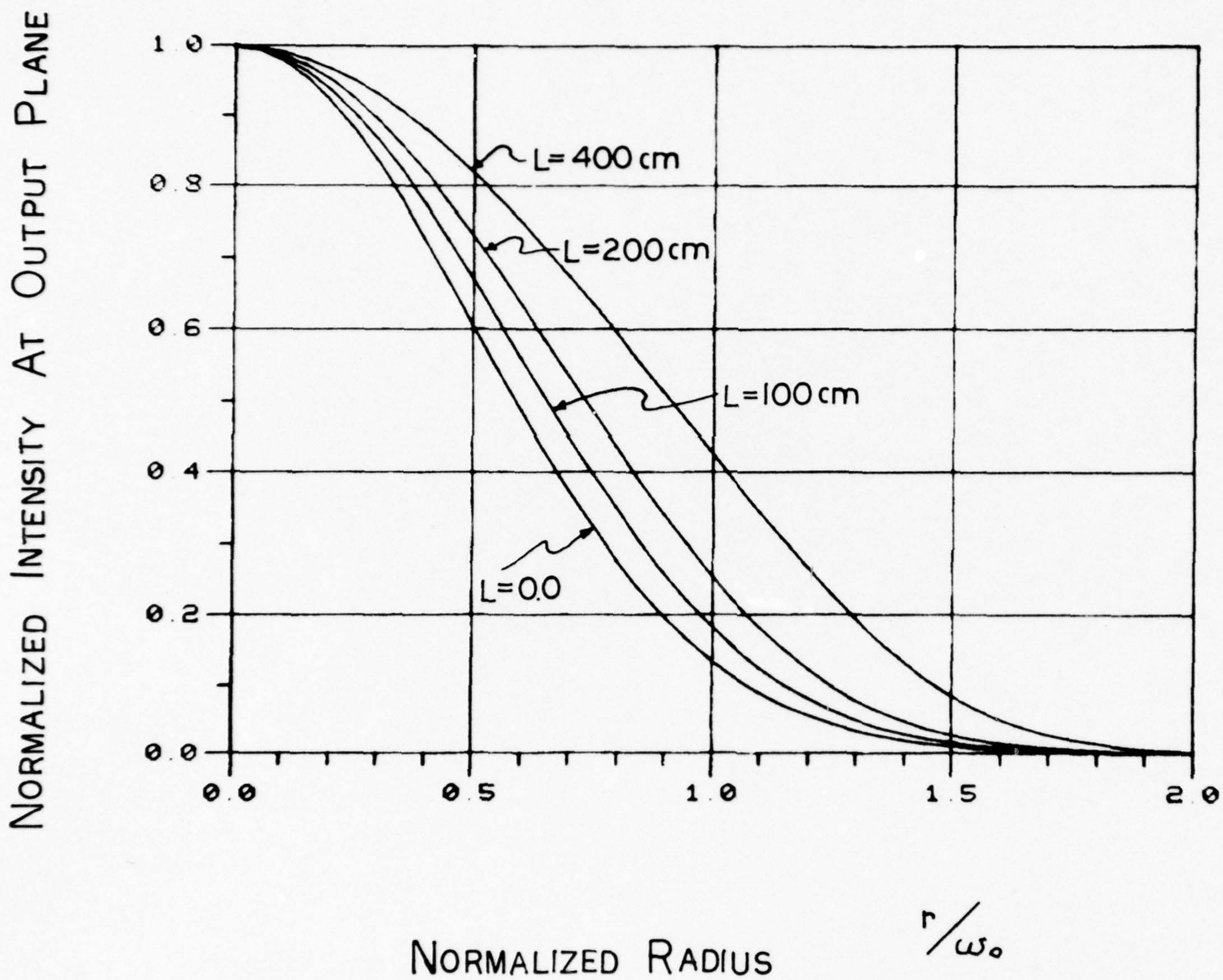

NORMALIZED INTENSITY AT OUTPUT PLANE
1.0
0.8
0.6
0.4
0.2
0.0
0.0
0.5
1.0
1.5
2.0
L=400 cm
L=200 cm
L=100 cm
L=0.0
NORMALIZED RADIUS
r/ω₀

FIG. 17

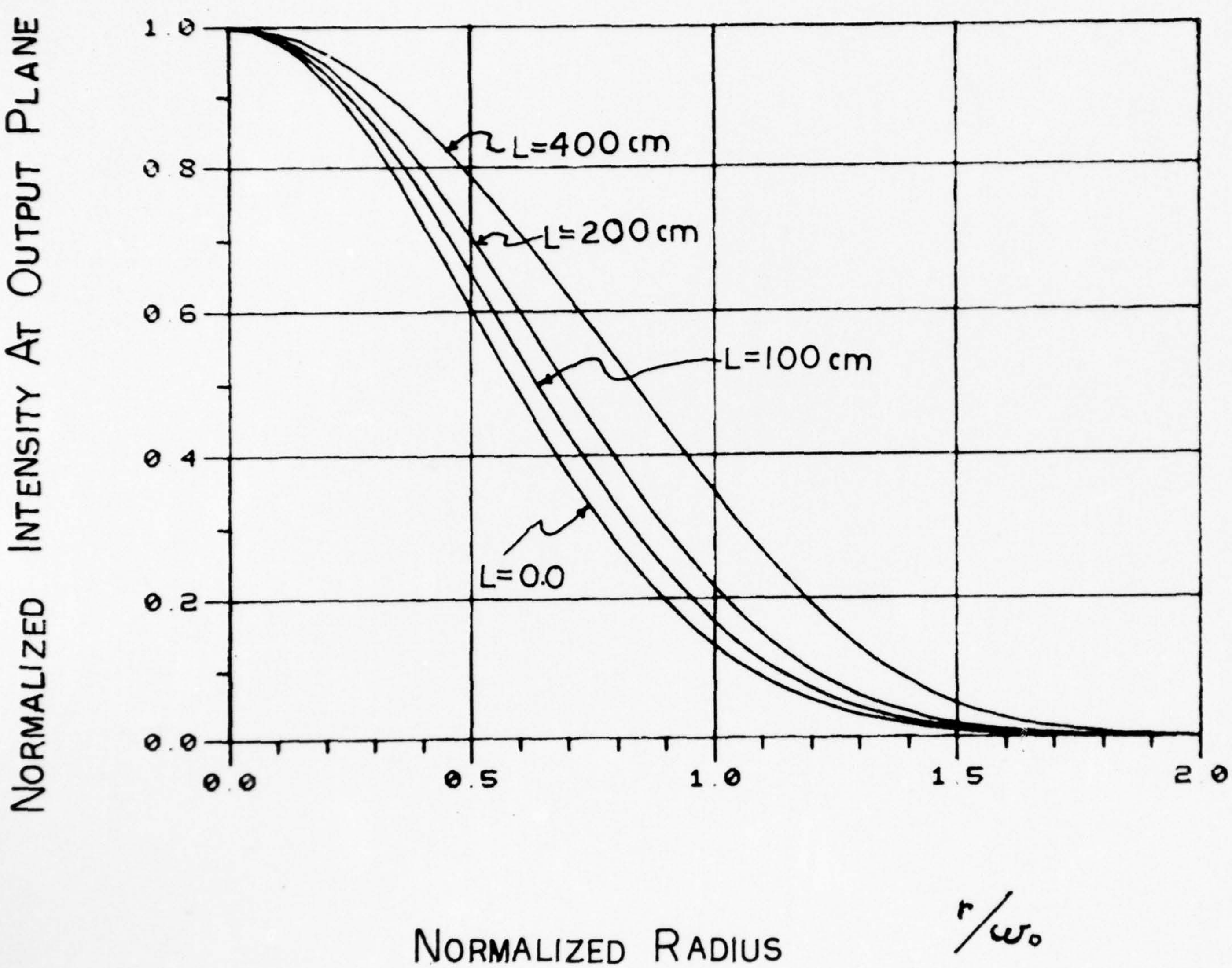
NORMALIZED INTENSITY AT OUTPUT PLANE
1.0
0.8
0.6
0.4
0.2
0.0
0.0
0.5
1.0
1.5
2.0
L=400 cm
L=200 cm
L=100 cm
L=0.0
NORMALIZED RADIUS
r/ω₀

FIG. 18

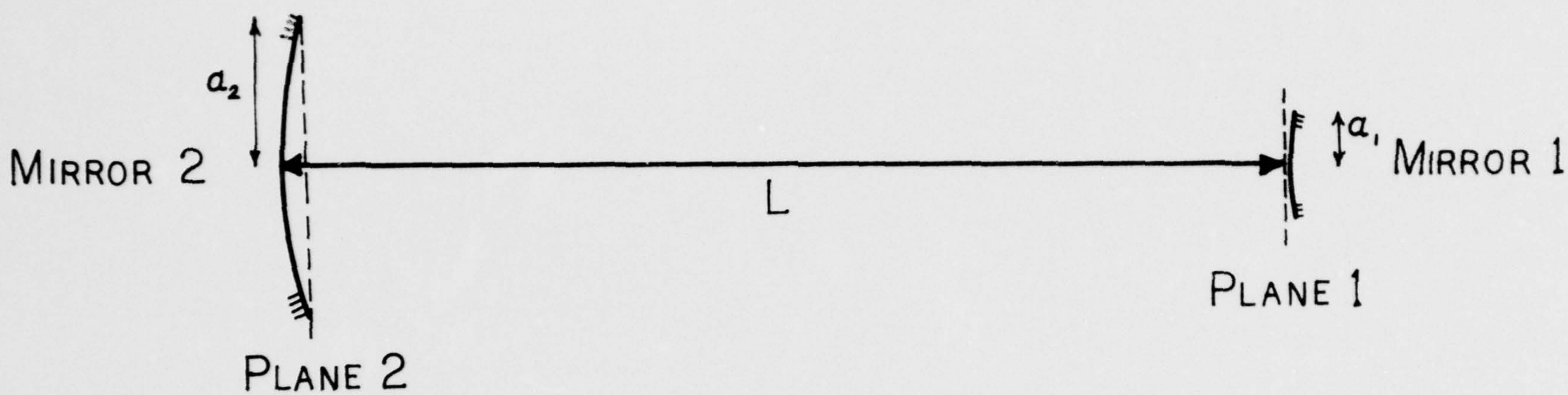

FIG. 19

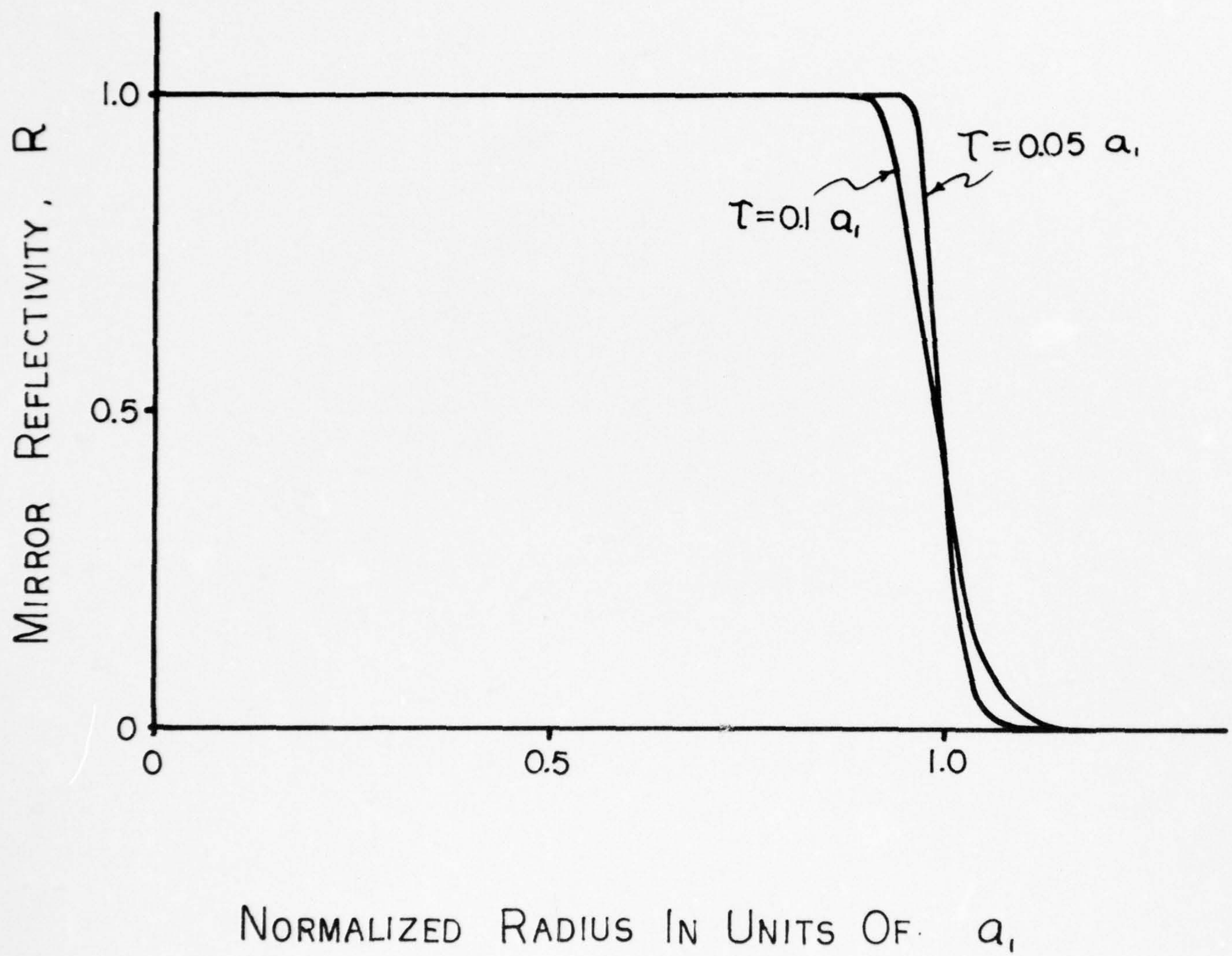

1.0
0.5
0
0
0.5
1.0
Mirror Reflectivity, R
τ=0.1 a₁
τ=0.05 a₁
Normalized Radius In Units Of a₁

Fig. 20

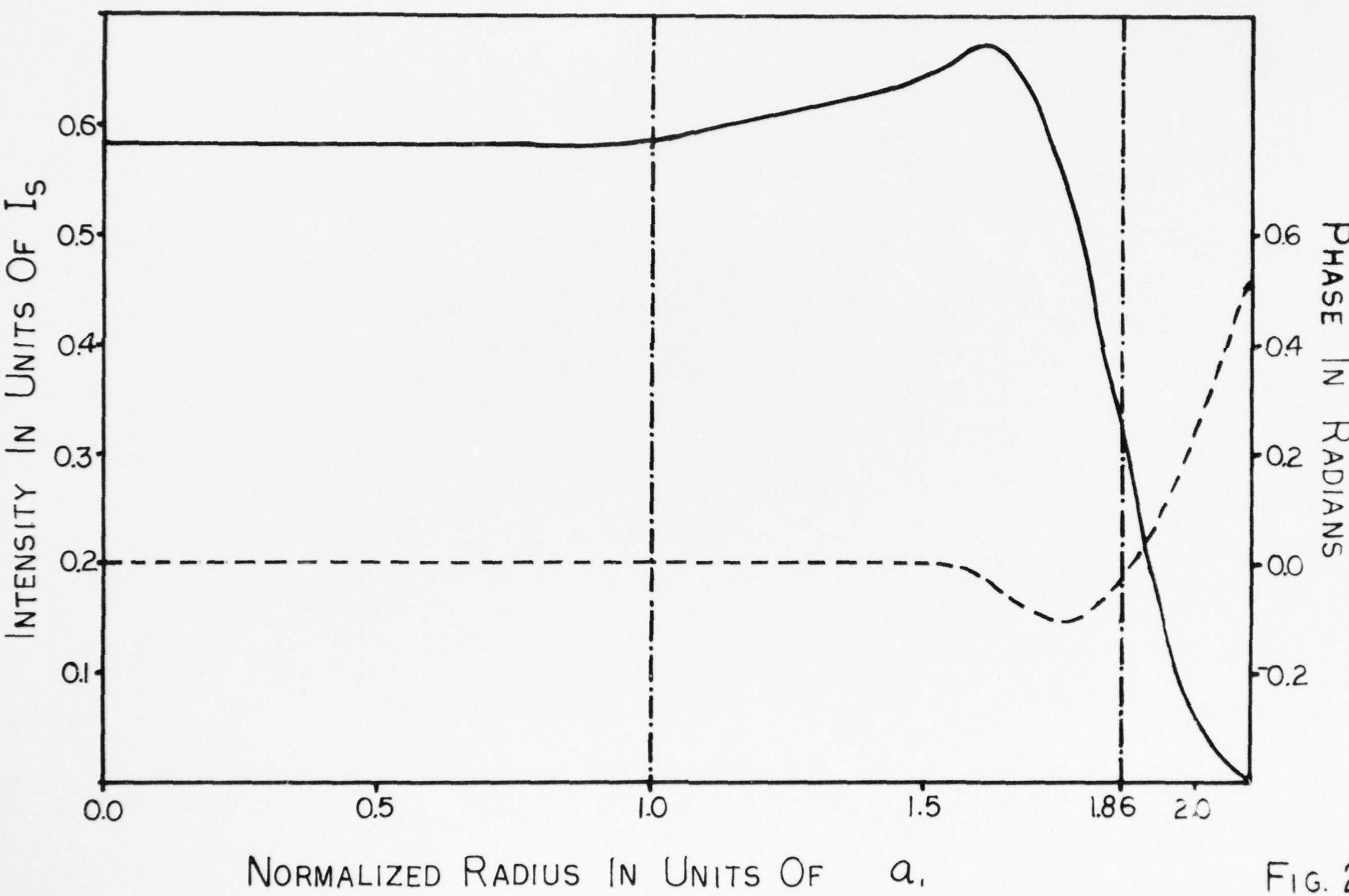
Intensity In Units Of I_S
0.6
0.5
0.4
0.3
0.2
0.1
Phase In Radians
0.6
0.4
0.2
0.0
-0.2
0.0
0.5
1.0
1.5
1.86
2.0
Normalized Radius In Units Of a,

Fig. 21

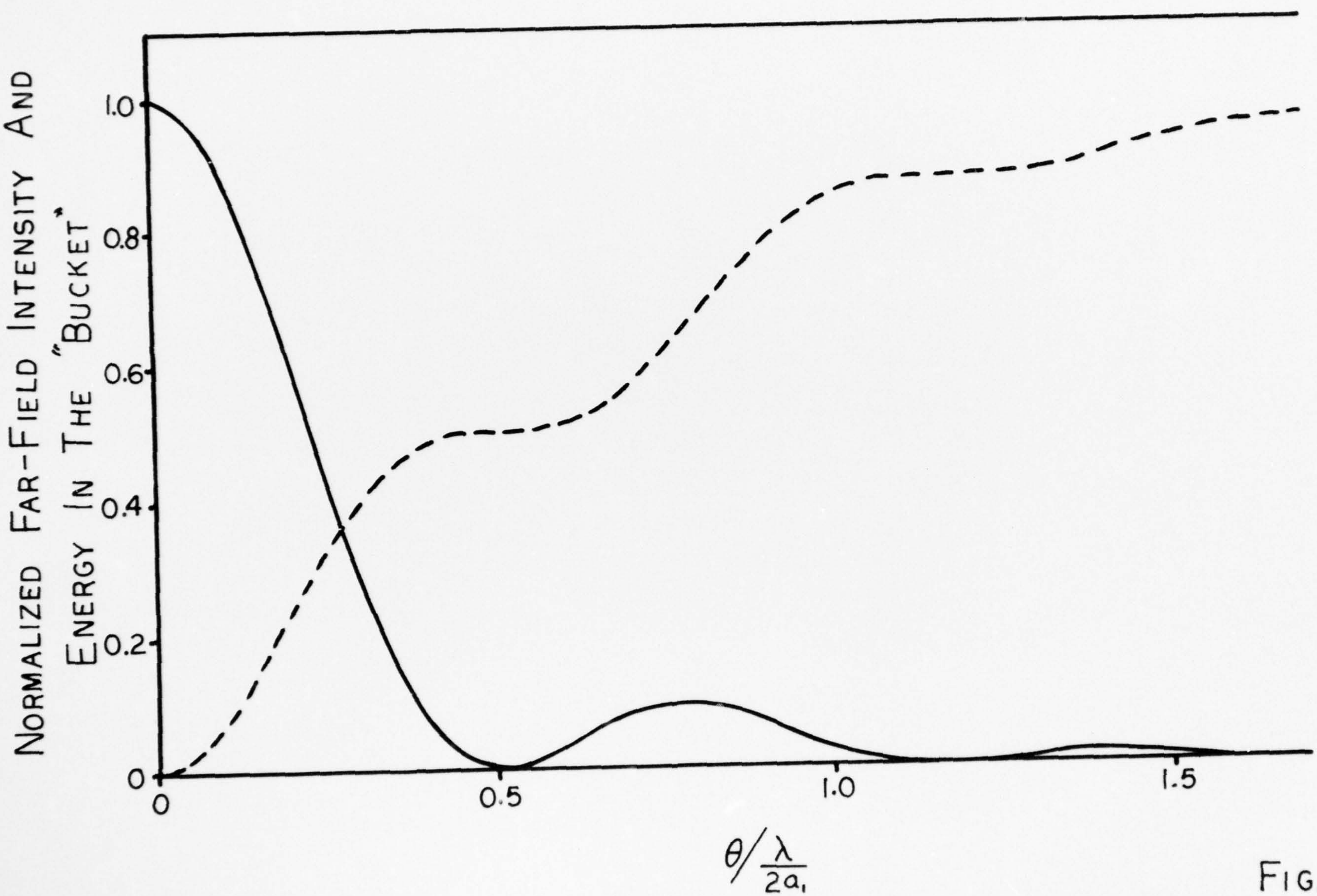

Normalized Far-Field Intensity And
Energy In The "Bucket"
1.0
0.8
0.6
0.4
0.2
0
0
0.5
1.0
1.5
$\theta / \frac{\lambda}{2a_1}$

Fig. 22

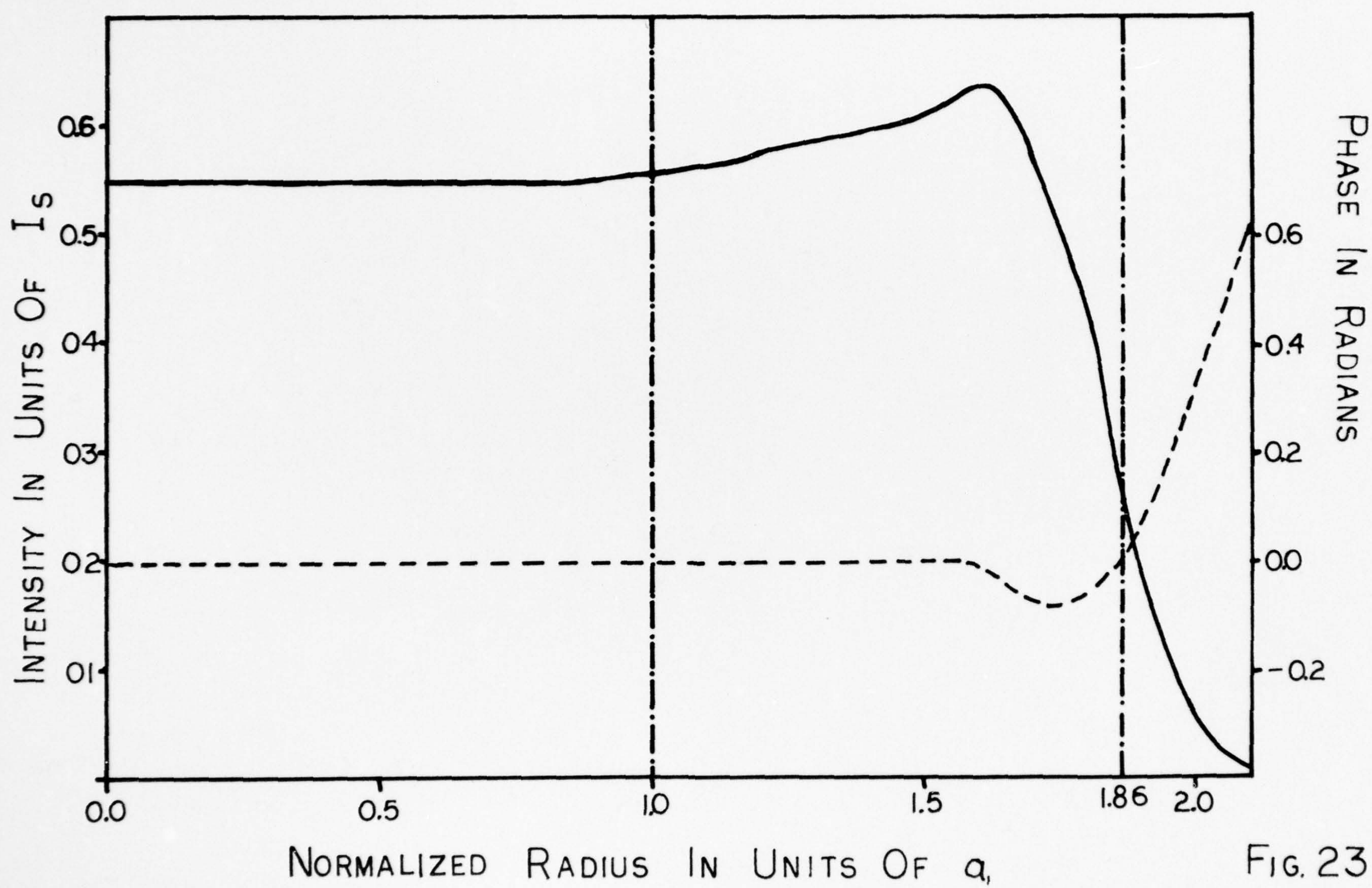

Intensity In Units Of I_s
0.6
0.5
0.4
0.3
0.2
0.1
Phase In Radians
0.6
0.4
0.2
0.0
-0.2
0.0
0.5
1.0
1.5
1.86
2.0
Normalized Radius In Units Of a_1

FIG. 23

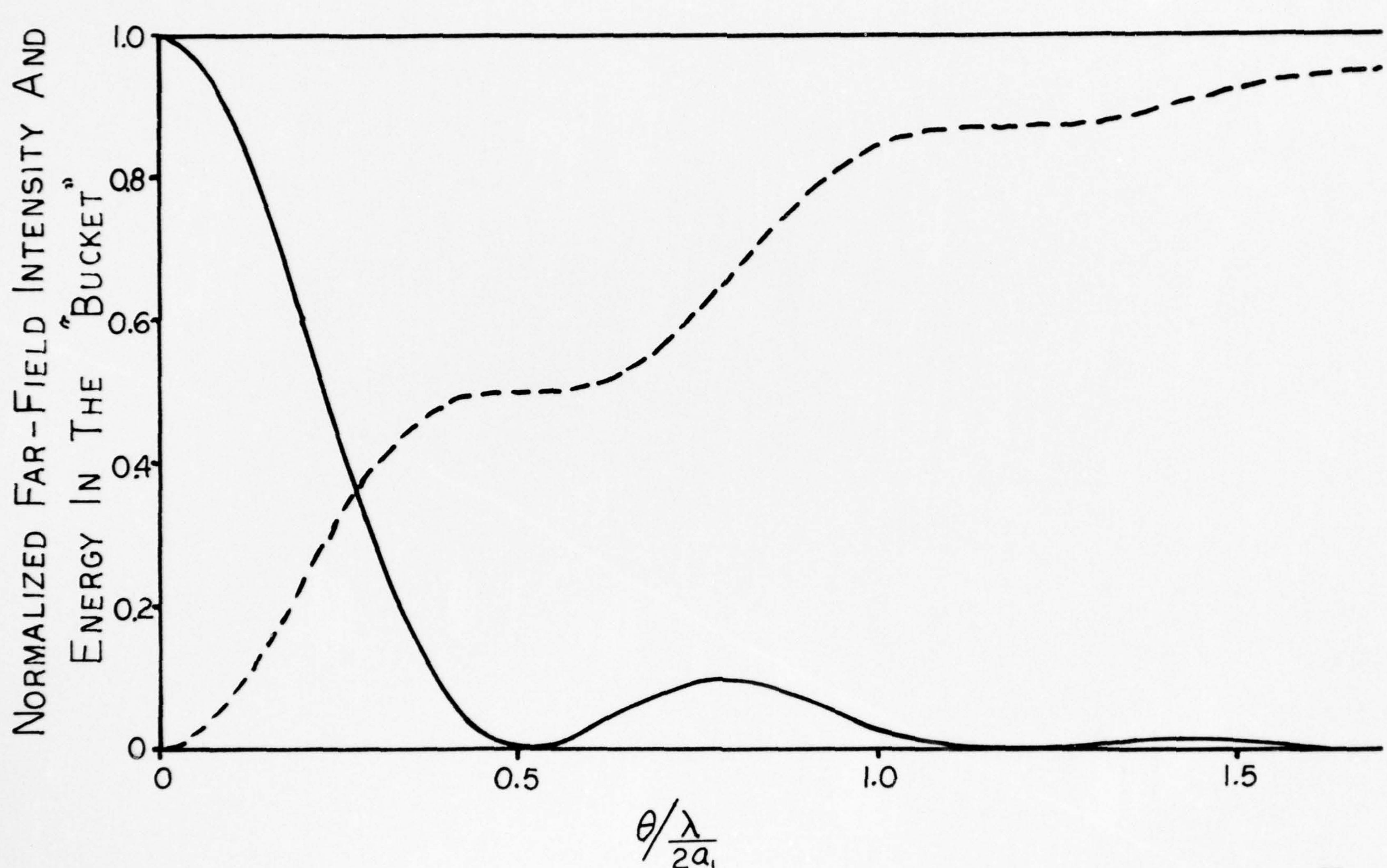

Normalized Far-Field Intensity And
Energy In The "Bucket"
1.0
0.8
0.6
0.4
0.2
0
0
0.5
1.0
1.5
$\theta / \frac{\lambda}{2a_1}$

Fig. 24

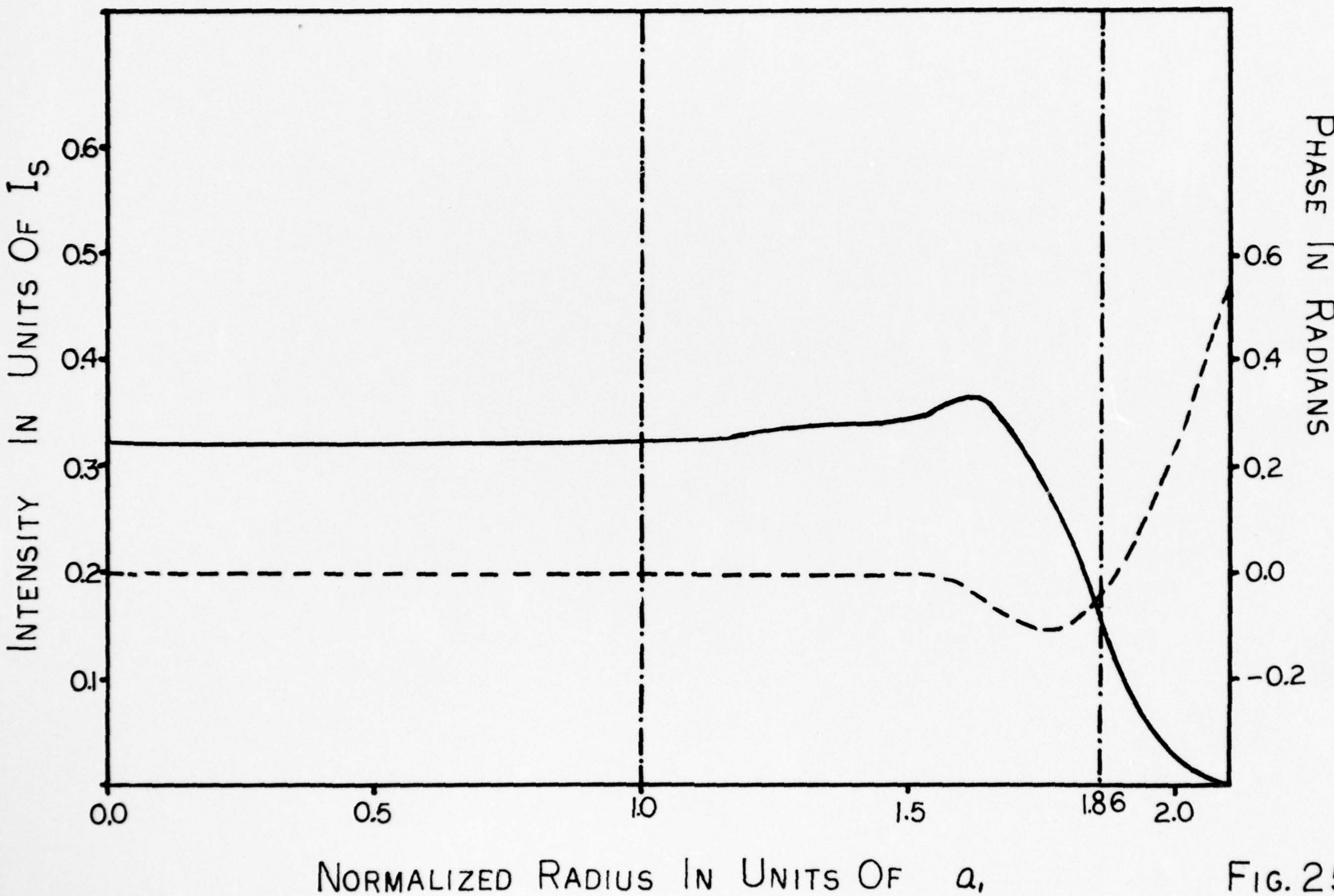
Intensity In Units Of I_s
0.6
0.5
0.4
0.3
0.2
0.1
Phase In Radians
0.6
0.4
0.2
0.0
-0.2
0.0
0.5
1.0
1.5
1.86
2.0
Normalized Radius In Units Of a_1

Fig. 25

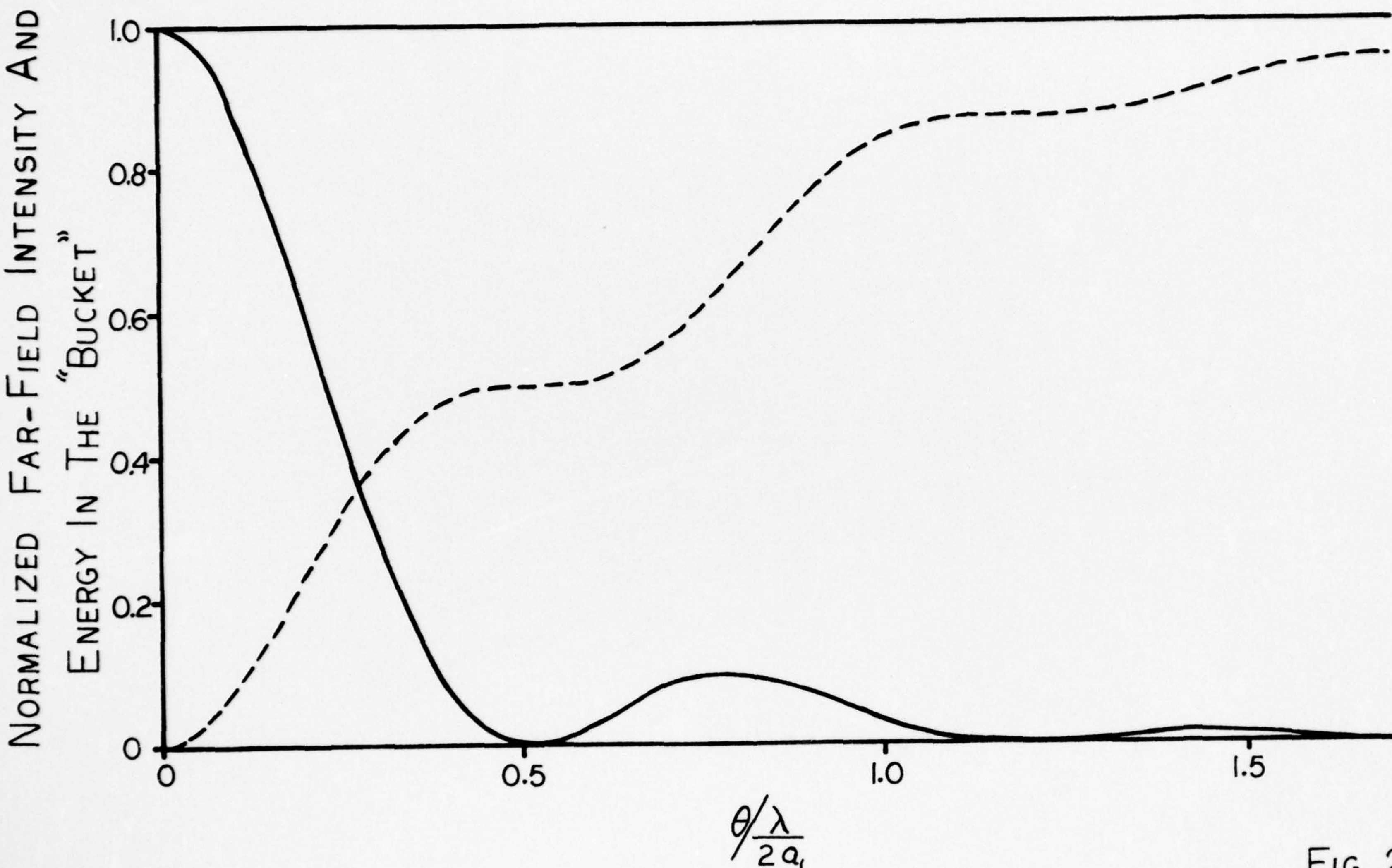

Normalized Far-Field Intensity And
Energy In The "Bucket"
1.0
0.8
0.6
0.4
0.2
0
0
0.5
1.0
1.5
$\theta / \frac{\lambda}{2a_1}$

Fig. 26

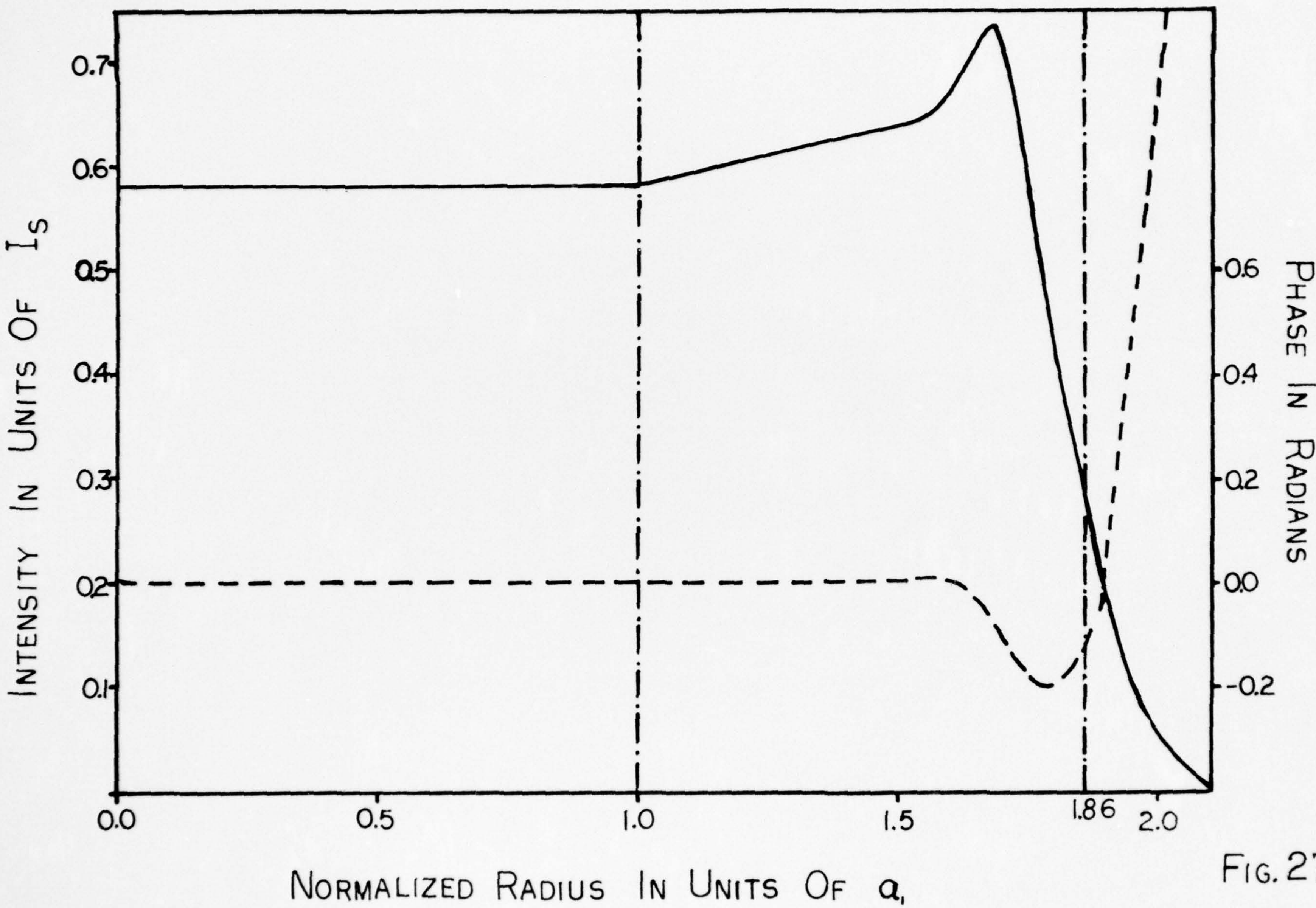
0.7
0.6
0.5
0.4
0.3
0.2
0.1
Intensity In Units Of I_s
0.6
0.4
0.2
0.0
-0.2
Phase In Radians
0.0
0.5
1.0
1.5
1.86
2.0
Normalized Radius In Units Of a_1

Fig. 27

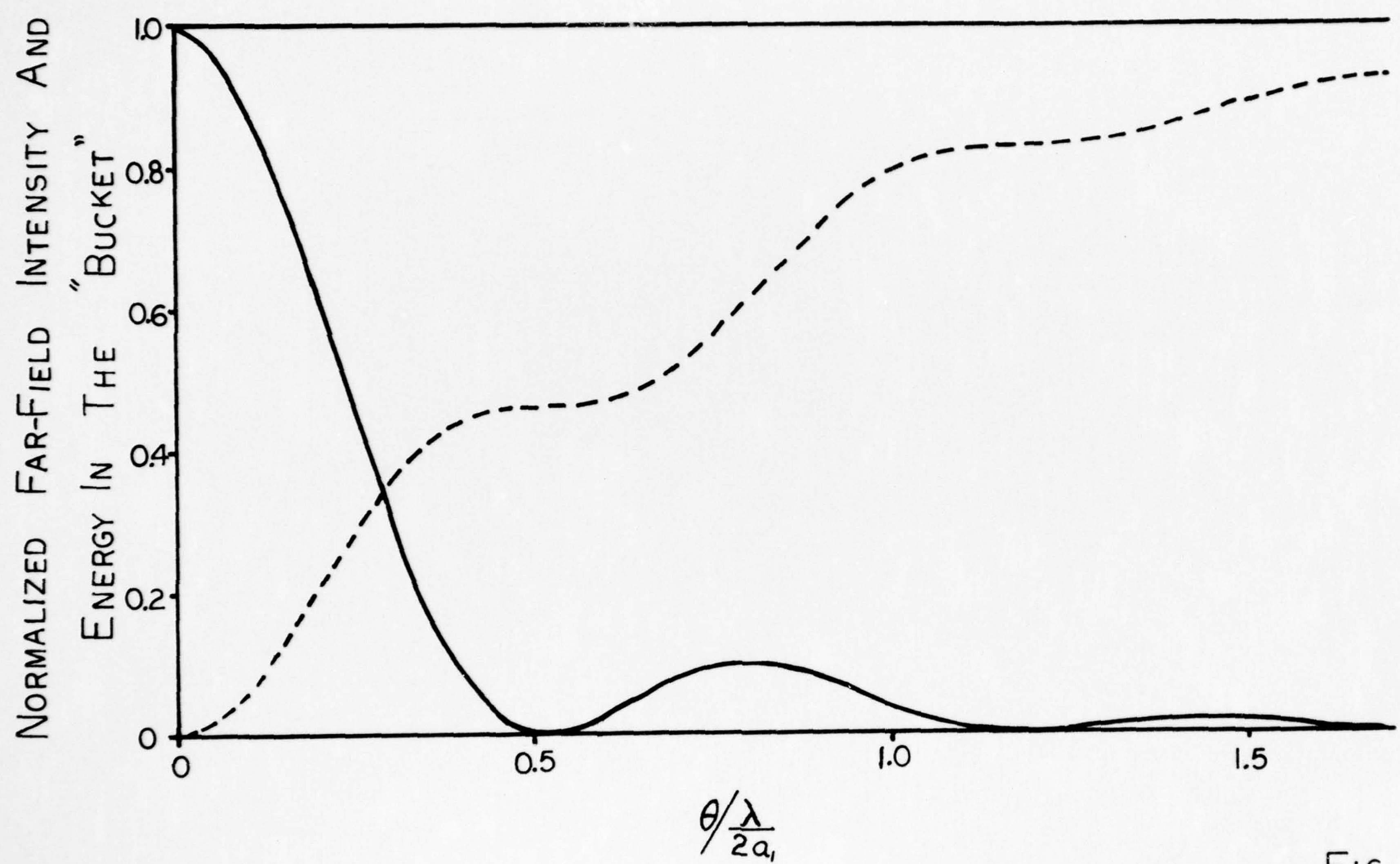
Normalized Far-Field Intensity And
Energy In The "Bucket"
1.0
0.8
0.6
0.4
0.2
0
0.5
1.0
1.5
$\theta / \frac{\lambda}{2a_1}$

FIG. 28

APPENDIX I

```
@ELT,IOL TPF$.CARD
ELT0T7 RLIB70 07/19-10:07:59-(,0)
000  @HDG  CYLINDERICALLY SYMMETRIC AMPLIFIER WITH SATURATED GAIN
000  @FOR,IS GAINAMPL,GAINAMPL
000        DIMENSION RIN(61), SINORM(61), SNORM(61)
000        COMMON GAIN, SIN, OMEGA, Z, NZ, NR, DZ
000        COMMON R(61), V(61), S(61)
000        COMMON RM(61), VM(61), SM(61), RP(61), VP(61), SP(61)
000        DO 99 NSET=1,1
000  C
000  C   NSET SPECIFIES THE NUMBER OF CALCULATIONS
000  C
000        READ (5,101) GAINSS, SIN, OMEGA, W0, ZZ, NZ, NR
000    101 FORMAT(5F14.5,2I5)
000  C
000  C   GAINSS IS THE SMALL SIGNAL GAIN PER CM
000  C   SIN IS THE INCIDENT INTENSITY IN UNITS OF THE SATURATION INTENSITY
000  C   OMEGA IS THE PARAMETER FOR THE AMOUNT OF SHIFT FROM RESONANCE
000  C   W0 IS THE INCIDENT BEAM SPOT SIZE IN CM
000  C   ZZ IS THE LASER LENGTH IN CM
000  C   NZ IS THE NUMBER OF POINTS ALONG THE Z AXIS
000  C   NR IS THE NUMBER OF POINTS ALONG THE RADIAL DIRECTION
000  C
000        DIFLGT=2.*3.14159*W0*W0/0.00106
000        GAIN=GAINSS*DIFLGT
000        Z=ZZ/DIFLGT
000  C
000  C   DIFLGT IS THE DIFFRACTION LENGTH
000  C   GAIN IS THE SMALL SIGNAL GAIN TIMES THE DIFFRACTION LENGTH
000  C   Z IS THE LASER LENGTH IN UNITS OF L (THE DIFFRACT+ON LENGTH)
000  C   R IS THE BEAM RADIUS IN UNITS OF W0 (THE INCIDENT BEAMS SPOT SIZE)
000  C
000        WRITE (6,130)
000    130 FORMAT(1H1)
000        WRITE(6,102) GAINSS
000        WRITE(6,103) SIN
000        WRITE(6,104) OMEGA
000        WRITE(6,105) W0
000        WRITE(6,106) ZZ
000        WRITE(6,107) NZ
000        WRITE(6,108) NR
000        WRITE(6,109) GAIN
000        WRITE(6,110) Z
000    102 FORMAT('0',10X,'SMALL SIGNAL GAIN PER CM =',F10.3,)
000    103 FORMAT('0',10X,'INCIDENT INTENSITY=',F15.5,
000       A        IN UNITS OF SATURATION INTENSITY')
000    104 FORMAT('0',10X, 'THE AMOUNT OF SHIFT FROM RESONANCE =',F15.5)
000    105 FORMAT('0',10X, 'THE BEAM SPOT SIZE =',F10.4,'  CM')
000    106 FORMAT('0',10X,'LENGTH OF THE AMPLIFIER =',F10.4,'  CM')
000    107 FORMAT('0',10X,'NUMBER OF POINTS ALONG Z AXIS =',I5)
000    108 FORMAT('0',10X,'NUMBER OF POINTS ALONG RADIAL DIRECTION =',I5)
000    109 FORMAT('0',10X,'SMALL SIGNAL GAIN TIMES DIFFRACTION LENGTH =',
000       A   F15.5)
000    110 FORMAT('0',10X,'LENGTH OF THE AMPLIFIER =',F15.5,
000       A   '   IN UNITS OF DIFFRACTION LENGTH')
000        DZ=Z/NZ
000        DO 10 J=1,NR
```

```
000          RIN(J)=2.*(J-1)/(NR-1)
000          SINORM(J)=EXP(-2.*RIN(J)**2)
000          R(J)=RIN(J)
000          V(J)=0.0
000          S(J)=SIN*SINORM(J)
000     C
000     C    INITIAL BEAM IS GAUSSIAN WITH PEAK INTENSITY SIN, SPOT SIZE W0
000     C    V IS THE RAY SLOP
000     C    S IS THE BEAM INTENSITY
000     C
000          RM(J)=R(J)
000          VM(J)=V(J)
000          SM(J)=S(J)
000       10 CONTINUE
000          DO 60 I=1,NZ
000          CALL PROPAG
000     C
000     C    PROPAG CALCULATS RP, VP, SP IN THE (I+1)TH PLANE FROM R, V, S IN
000     C    THE ITH PLANE AND RM, VM, SM IN THE (I-1)TH PLANE
000     C
000          DO 50 J=1,NR
000          RM(J)=R(J)
000          VM(J)=V(J)
000          SM(J)=S(J)
000          R(J)=RP(J)
000          V(J)=VP(J)
000          S(J)=SP(J)
000       50 CONTINUE
000          ITEST=I/100.
000          ITEST=I-100*ITEST
000          IF(ITEST.EQ.0) GO TO 55
000          GO TO 60
000       55 ZP=I*DZ*DIFLGT
000          WRITE(6,130)
000          WRITE(6,140) ZP, I
000      140 FORMAT(3X,'THE DISTANCE ALONG THE AMPLIFIER =',F10.4,'  CM',10X,
000         A    'THE NUMBER OF POINTS ALONG THE AMPLIFIER =',I5)
000          WRITE(6,120)
000          WRITE(6,120)
000      120 FORMAT(1H0)
000          WRITE(6,111)
000          WRITE(6,112)
000      111 FORMAT('0',20X,1HR,10X, 8HINCIDENT,9X,6HRADIAL,10X,
000         A    4HBEAM,10X,4HBEAM,9X,10HNORMALIZED)
000      112 FORMAT(32X,7HPROFILE,9X,8HDISTANCE,9X,5HSLOPE,9X,9HINTENSITY,4X,
000         A    9HINTENSITY)
000          WRITE(6,120)
000          DO 70 J=1,NR
000          SNORM(J)=S(J)/S(1)
000          WRITE(6,150) J, RIN(J), SINORM(J), R(J), V(J), S(J), SNORM(J)
000       70 CONTINUE
000      150 FORMAT(I10,6F15.5)
000       60 CONTINUE
000          WRITE(6,120)
000       99 CONTINUE
000          STOP
000          END
```

```
000    @FOR,IS PROPAG,PROPAG
000          SUBROUTINE PROPAG
000          COMMON GAIN, SIN, OMEGA, Z, NZ, NR, DZ
000          COMMON R(61), V(61), S(61)
000          COMMON RM(61), VM(61), SM(61), RP(61), VP(61), SP(61)
000          DIMENSION RDZ(61), VDZ(61), SDZ(61)
000          DIMENSION RPB(61),SPB(61),VPB(61),RPBDZ(61),SPBDZ(61),VPBDZ(61)
000          CALL GRADNT(R,S,V,RDZ,SDZ,VDZ)
000    C
000    C   GRADNT CALCULATES DERIVATIVES DR/DZ, DS/DZ AND DV/DZ AT GIVEN
000    C   R, S AND V
000    C
000          DO 10 J=1,NR
000          RPB(J)=RM(J)+2.*RDZ(J)*DZ
000          SPB(J)=SM(J)+2.*SDZ(J)*DZ
000          VPB(J)=VM(J)+2.*VDZ(J)*DZ
000       10 CONTINUE
000    C
000    C   RPB, SPB AND VPB ARE PREDICTED VALUES AT THE (I+1)TH PLANE
000    C
000          NITER=0
000       15 CALL GRADNT(RPB,SPB,VPB,RPBDZ,SPBDZ,VPBDZ)
000          NITER=NITER+1
000          DO 20 J=1,NR
000          RP(J)=R(J)+0.5*(RPBDZ(J)+RDZ(J))*DZ
000          SP(J)=S(J)+0.5*(SPBDZ(J)+SDZ(J))*DZ
000          VP(J)=V(J)+0.5*(VPBDZ(J)+VDZ(J))*DZ
000       20 CONTINUE
000          DO 30 J=1,NR
000          IF(ABS(RP(J)-RPB(J)).GT.0.00001) GO TO 35
000          IF(ABS(SP(J)-SPB(J)).GT.0.00010) GO TO 35
000          IF(ABS(VP(J)-VPB(J)).GT.0.00001) GO TO 35
000       30 CONTINUE
000    C
000    C   RP, SP, VP ARE CALCULATED, IF THEY ARE DIFFERENT FROM RPB, SPB, VPB,
000    C   WE REPEAT THE CALCULATION WITH RP, SP, VP FOR RPB, SPB, VPB
000    C
000          GO TO 50
000       35 IF(NITER.GT.10) GO TO 50
000          DO 40 J=1,NR
000          RPB(J)=RP(J)
000          SPB(J)=SP(J)
000          VPB(J)=VP(J)
000       40 CONTINUE
000          GO TO 15
000       50 CONTINUE
000          RETURN
000          END
000    @FOR,IS GRADNT,GRADNT
000          SUBROUTINE GRADNT (R,S,V,RDZ,SDZ,VDZ)
000          COMMON GAIN, SIN, OMEGA, Z, NZ, NR, DZ
000          DIMENSION R(61), S(61), V(61), RDZ(61), SDZ(61), VDZ(61)
000          DIMENSION DV(61), SLN(61), G(61), DG(61), P(61), DP(61)
000          DO 10 J=1,NR
000          SLN(J)=ALOG(S(J))
000       10 CONTINUE
000          NRM=NR-1
```

```
      CALL DRITIV(R(1),R(2),R(3),V(1),V(2),V(3),R(1),DV(1))
      G(1)=0.0
      DO 11 J=2,NRM
      CALL DRITIV(R(J-1),R(J),R(J+1),V(J-1),V(J),V(J+1),R(J),DV(J))
      CALL DRITIV(R(J-1),R(J),R(J+1),SLN(J-1),SLN(J),SLN(J+1),R(J),G(J))
   11 CONTINUE
      CALL DRITIV(R(NR-2),R(NR-1),R(NR),V(NR-2),V(NR-1),V(NR),R(NR),
     A   DV(NR))
      CALL DRITIV(R(NR-2),R(NR-1),R(NR),SLN(NR-2),SLN(NR-1),SLN(NR),
     A   R(NR),G(NR))
      CALL DRITIV(R(1),R(2),R(3),G(1),G(2),G(3),R(1),DG(1))
      P(1)=G(1)*G(1)/2.+2.*DG(1)+2.*GAIN*OMEGA/(1.+OMEGA**2+S(1))
      DO 21 J=2,NRM
      CALL DRITIV(R(J-1),R(J),R(J+1),G(J-1),G(J),G(J+1),R(J),DG(J))
      P(J)=G(J)*G(J)/2.+DG(J)+G(J)/R(J)
     A   +2.*GAIN*OMEGA/(1.+OMEGA**2+S(J))
   21 CONTINUE
      CALL DRITIV(R(NR-2),R(NR-1),R(NR),G(NR-2),G(NR-1),G(NR),R(NR),
     A   DG(NR))
      P(NR)=G(NR)*G(NR)/2.+DG(NR)+G(NR)/R(NR)
     A   +2.*GAIN*OMEGA/(1.+OMEGA**2+S(NR))
      CALL DRITIV(R(1),R(2),R(3),P(1),P(2),P(3),R(1),DP(1))
      DO 31 J=2,NRM
      CALL DRITIV(R(J-1),R(J),R(J+1),P(J-1),P(J),P(J+1),R(J),DP(J))
   31 CONTINUE
      CALL DRITIV(R(NR-2),R(NR-1),R(NR),P(NR-2),P(NR-1),P(NR),R(NR),
     A   DP(NR))
      RDZ(1)=V(1)
      SDZ(1)=GAIN*S(1)/(1.+OMEGA**2+S(1))-2.*S(1)*DV(1)
      VDZ(1)=0.0
      DO 41 J=2,NR
      RDZ(J)=V(J)
      SDZ(J)=GAIN*S(J)/(1.+OMEGA**2+S(J))-S(J)*DV(J)-S(J)*V(J)/R(J)
      VDZ(J)=0.25*DP(J)
   41 CONTINUE
      RETURN
      END
@FOR,IS DRIT,V,DRITIV
      SUBROUTINE DRITIV (X1,X2,X3,Y1,Y2,Y3,X,DYDX)
C
C   GIVEN Y1 AT X1, Y2 AT X2, Y3 AT X3 IT CALCULATES DY/DX AT GIVEN X
C
      D=(X1-X2)*(X2-X3)*(X3-X1)
      B=(Y1*(X2*X2-X3*X3)+Y2*(X3*X3-X1*X1)+Y3*(X1*X1-X2*X2))/D
      C=-(Y1*(X2-X3)+Y2*(X3-X1)+Y3*(X1-X2))/D
      DYDX=B+2.*C*X
      RETURN
      END
@XQT
        0.01          0.25          0.5          2.5          400.        400   41

END ELT.

@FIN
```